



Published in final edited form as:

J Med Chem. 2013 March 28; 56(6): 2385–2405. doi:10.1021/jm301709s.

Non-nucleoside Inhibitors of BasE, An Adenylating Enzyme in the Siderophore Biosynthetic Pathway of the Opportunistic Pathogen *Acinetobacter baumannii*

João Neres^{1,†}, Curtis A. Engelhart^{1,2}, Eric J. Drake³, Daniel J. Wilson¹, Peng Fu¹, Helena I. Boshoff⁴, Clifton E. Barry 3rd⁴, Andrew M. Gulick³, and Courtney C. Aldrich^{1,*}

¹Center for Drug Design, Academic Health Center, University of Minnesota, Minneapolis, Minnesota 55455, United States

²Department of Medicinal Chemistry, University of Minnesota, Minneapolis, Minnesota 55455, United States

³Hauptman-Woodward Institute and Department of Structural Biology, University at Buffalo, Buffalo, New York 14203-1102, United States

⁴Tuberculosis Research Section, National Institute of Allergy and Infectious Diseases, Bethesda, Maryland 20892, United States

Abstract

Siderophores are small-molecule iron chelators produced by bacteria and other microorganisms for survival under iron limiting conditions, such as found in a mammalian host. Siderophore biosynthesis is essential for the virulence of many important Gram-negative pathogens including *Acinetobacter baumannii*, *Klebsiella pneumoniae*, *Pseudomonas aeruginosa*, and *Escherichia coli*. We performed high-throughput screening of against BasE, which is involved in siderophore biosynthesis in *A. baumannii* and identified 6-phenyl-1-(pyridin-4-ylmethyl)-1*H*-pyrazolo[3,4-*b*]pyridine-4-carboxylic acid **15**. Herein we report the synthesis, biochemical, and microbiological evaluation of a systematic series of analogues of the HTS hit **15**. Analogue **67** is the most potent analogue with a K_D of 2 nM against BasE. Structural characterization of the inhibitors with BasE reveal they bind in a unique orientation in the active site occupying all three substrate binding sites, and thus can be considered multisubstrate inhibitors. These results provide a foundation for future studies aimed at both increasing enzyme potency and antibacterial activity.

Introduction

The increase of antibacterial resistance coupled with the lack of new antibiotics is cause for great concern.^{1, 2} This is highlighted by the Gram-negative bacteria *Acinetobacter baumannii*, an opportunistic organism that has emerged over the last couple of decades as one of the most insidious pathogens.³ *A. baumannii* now accounts for more than 10% of hospital-acquired infections and is the leading cause of wound infections in soldiers in Iraq and Afghanistan.^{4, 5} Additionally, up to 30% of *A. baumannii* isolates in intensive care units

*CORRESPONDING AUTHOR FOOTNOTE. To whom correspondence should be addressed. Phone 612-625-7956. Fax 612-626-5173. aldri015@umn.edu.

[†]Present address: Global Health Institute, École Polytechnique Fédérale de Lausanne, 1015 Lausanne, Switzerland. joao.neres@epfl.ch.

Supporting Information Available: The synthetic procedures and characterization data for compounds **23–25**, **27–28**, **37–62**, and **64–92** as well as representative ¹H and ¹³C NMR spectra for **15**, **16**, **17**, **18**, **19**, **21**, **22**, **37**, **60**, **63**, **91**, **94**, and **98** can be found in the Supporting Information. This material is available free of charge via the Internet at <http://pubs.acs.org>.

are resistant to almost all known antibiotics including the β -lactams, fluoroquinolones, aminoglycosides, and tetracyclines.⁵ According to the MYSTIC susceptibility data from 15 North American medical centers, acinetobacter sensitivity is now below 60% for ceftazidime, cefepime, piperacillin/tazobactam, meropenem, imipenem, aztreonam, and gentamicin.⁶ Comparative genomic studies of *A. baumannii* identified an unprecedented 86-kb cluster of 45 resistance genes in one particular strain.^{7, 8} The prevalence of the multidrug resistance (MDR) phenotype among Gram-negative pathogens including *A. baumannii* has led infectious disease physicians to reintroduce the colistins and polymyxins.⁹ These related cationic lipopeptides were first introduced in the 1950's, but their use had been largely curtailed by the 1980's as a result of their considerable nephrotoxicity.¹⁰ *A. baumannii* clinical isolates have been reported that are no longer susceptible to these antibiotics of last resort.¹⁰ It is astonishing to think that we may soon enter an era when antibiotic therapy is unavailable for previously treatable infections.

All bacteria with the exception of *Borrelia burgdorferi*¹¹ require micromolar levels of iron ($\text{Fe}^{2+}/\text{Fe}^{3+}$) for growth since iron serves as a cofactor in numerous biochemical processes.¹² However, the concentrations of iron in serum and human body fluids is approximately 10^{-24} M. The extraordinarily low concentration of free iron provides innate immunity to bacterial infections and is a result of the insolubility of iron (III) under aerobic conditions and the sequestration of the remaining free iron by the iron-binding proteins such as transferrin and lactoferrin. Many pathogens like *A. baumannii* overcome this iron limitation via the synthesis of siderophores, which are small molecule high-affinity iron-chelators secreted by bacteria and reimported from the external milieu after successfully chelating non-heme host iron (Figure 1).¹²⁻¹⁵ The critical role that siderophores play in virulence has been demonstrated in *A. baumannii*,¹⁶ as well as in numerous other significant Gram-negative pathogens including *Klebsiella pneumoniae*,¹⁷ *Pseudomonas aeruginosa*,¹⁸ and *Escherichia coli*.¹⁹ Siderophores are also critical for the virulence of many Gram-positive bacteria including *Bacillus anthracis*,²⁰ *Staphylococcus aureus*,²¹ and the acid fast *Mycobacterium tuberculosis*.²² Consequently, inhibition of siderophore biosynthesis represents a promising new strategy for antibacterial drug development; an approach that is further bolstered by the observation that many bactericidal antibiotics ultimately operate through disruption of bacterial iron homeostasis and generation of reactive oxygen species (ROS).^{23, 24}

A. baumannii produces acinetobactin, a mixed ligand siderophore containing a catechol and imidazole for iron coordination.^{25, 26} The biosynthesis of acinetobactin is initiated by BasE that activates and loads 2,3-dihydroxybenzoic acid (DHB) onto a nonribosomal peptide synthetase (NRPS) pathway comprised of four other proteins (BasF, BasD, BasA, and BasB).^{27, 28} This assembly line of proteins condenses DHB, L-threonine, and *N*-hydroxyhistamine to afford preacinetobactin **11**, which spontaneously rearranges to acinetobactin **1** (Figure 2).^{29, 30} BasE represents an ideal target since it does not possess a mammalian homologue, the protein has been biochemically and structurally characterized,³¹ and the functionally related aminoacyl t-RNA synthetases are validated antibiotic targets with mupirocin the first in class inhibitor.³² Homologues from other organisms as shown in Table 1 suggest inhibitors may also be useful to combat several significant bacterial pathogens.

BasE is an aryl acid adenylating enzyme (AAAE) and catalyzes the condensation of DHB **8** with ATP to form an acyl-adenylate intermediate **9**, whereby the carboxy group is activated as a mixed anhydride. Following liberation of pyrophosphate, BasE binds the phosphopantetheinylated aryl carrier protein (ArCP) domain of BasF to form a ternary complex and then catalyzes the transfer of the activated DHB onto the terminal thiol of the pantetheine moiety of BasF to provide thioester **10** (Figure 2).³³ AAAEs are members of the ANL superfamily of enzymes that contain a large N-terminal domain and a smaller C-

terminal domain with the active site located at the domain interface.³⁴ AAAs thus carry out two reactions, an adenylation and thioesterification, at the same active site. In the adenylation reaction, a catalytic lysine from the C-terminal subdomain coordinates the carboxylate substrate and directs nucleophilic attack on the α -phosphate of ATP. The enzyme then undergoes a $\sim 140^\circ$ rigid body rotation about a hinge residue (Lys437 in BasE), which allows the phosphopantetheine arm of the carrier domain to insert into the active-site for thioester formation.³⁴

5'-O-[N-(Salicyl)sulfamoyl]adenosine (Sal-AMS, **12**) and the related 5'-O-[N-(2,3-dihydroxybenzoyl)sulfamoyl]adenosine (2,3-DHB-AMS, **13**) are the first confirmed AAAE inhibitors of siderophore biosynthesis with potent nanomolar apparent K_i values against a range of AAAs including BasE, YbtE, and MbtA from *A. baumannii*, *Yersinia sp.*, and *M. tuberculosis*, respectively (Figure 3).^{31, 35–37} Sal-AMS and 2,3-DHB-AMS mimic the acyladenylate intermediate **9** (Figure 2) through replacement of the labile acylphosphate moiety with a stable acylsulfamate isostere. Sal-AMS displays impressive activity against the acid-fast Gram-positive *M. tuberculosis* with a minimum inhibitory concentration (MIC) of 0.39 μM under iron-deficient conditions. However, the antibacterial potency of Sal-AMS is more than 100 times weaker against Gram-negative *Y. pestis* and *Y. pseudotuberculosis* under the same conditions, despite possessing potent nanomolar enzyme inhibition of YbtE, the respective AAAE from these organisms.^{35, 38} Moreover, Sal-AMS and 2,3-DHB-AMS display no activity against other Gram-negative organisms including *A. baumannii*, *K. pneumoniae*, *E. coli*, and *P. aeruginosa* (unpublished results, Brian Beck, Laura Celia, ATCC). The reason for such a striking difference could be that the highly polar (ClogP ~ -2) and negatively charged nucleoside derivatives may prevent cellular uptake, although many other mechanisms of intrinsic resistance may be involved.

We have recently reported the discovery of a new class of potent non-nucleoside AAAE inhibitors through high-throughput screening (HTS) using a fluorescence polarization (FP) displacement assay with a fluorescent analogue of Sal-AMS (Fl-Sal-AMS, **14**) as a ligand.³⁹ The most potent hit discovered, pyrazolopyridine **15** (Figure 3) binds BasE with a submicromolar dissociation constant as determined independently by isothermal titration calorimetry and our FP assay.³⁹ Further kinetic characterization of **15** reveals it exhibits competitive inhibition with respect to both substrates 2,3-DHB and ATP.³¹ Herein we report the design, synthesis, biochemical, and biological evaluation of a systematic series of analogues of **15** that comprehensively explores the SAR of this promising scaffold. Structural information is also reported for the complexes of BasE with two of the most potent analogues of **15** as well as in vitro data demonstrating that deletion of *basE* in *A. baumannii* impairs growth under iron-deficient conditions.

Results

Chemistry

The structure of 6-phenyl-1-(pyridin-4-ylmethyl)-1H-pyrazolo[3,4-*b*]pyridine-4-carboxylic acid (**15**) discovered from high-throughput screening³⁹ can be divided into four domains for SAR purposes as depicted in Figure 4. This compound is part of a large compound library supplied by Enamine (Ukraine) and there is no literature available regarding its synthesis or any other properties.

For the synthesis of **15** and analogues, the key intermediate ethyl 6-oxo-1-(pyridin-4-ylmethyl)-1H-pyrazolo[3,4-*b*]pyridine-4-carboxylate **109** was initially prepared, as well as the *p*-methoxyphenyl (PMP) analogue **108** (Scheme 1). The methodology devised by Hohn⁴⁰ was used to synthesize the 1-aryl-1H-pyrazol-5-amines **104** and **105**, through the multicomponent condensation of acrylonitrile **101**, hydrazine, and the appropriate aryl

aldehydes to afford the intermediate imines **102** and **103**. These were not isolated but directly converted to the corresponding pyrazoles via base-promoted cyclization and subsequent redox isomerization. Pyridone annulation was accomplished in a two-step process involving condensation of **104** and **105** with diethyl oxalacetate to provide **106** and **107**, which were then cyclized to the respective 1*H*-pyrazolo[3,4-*b*]pyridones **108** and **109** by refluxing in glacial acetic acid using the procedure described by Dorn and Müller.⁴¹

Elaboration of intermediates **108–109** to the final C-6 aryl pyrazolopyridines requires activation of the tautomerizable pyridone carbonyl as a halide or pseudohalide followed by Suzuki coupling and ester hydrolysis. We initially began with PMP analogue **108** since this provides *p*-hydroxybenzyl and *p*-methoxybenzyl analogues **31–32**, and selective deprotection of the PMP moiety would allow access to a wide variety of analogues at N-1 by direct alkylation of the resultant free amino group. Chlorination (POCl₃) of **108** was not successful (not shown), but the triflate **110** was readily obtained using triflic anhydride and 2,6-di-*t*-butyl-4-methylpyridine as base (Scheme 2). Suzuki coupling of **110** with phenylboronic acid under standard Suzuki conditions furnished the intermediate **111**. Cleavage of the PMP group proceeded optimally in neat TFA at 70 °C to afford compound **112**. Alkylation of **112** with 4-(bromomethyl)pyridine under a variety of conditions was then attempted. Although the desired product **15** was obtained, the reaction was not regioselective and alkylation occurred at both N-1 and N-2 of the pyrazole, leading to poor yields of the desired product (not shown). The intermediates **111** and **112** were readily hydrolyzed with NaOH in THF–H₂O at room temperature providing compounds **31** and **36**. The *p*-methoxy group of **111** was hydrolyzed using boron trifluoride-dimethyl sulfate complex, yielding the *p*-hydroxybenzyl analogue **32**. Buchwald-Hartwig coupling of triflate **110** with aniline followed by hydrolysis of the ethyl ester furnished the phenylamino analogue **100**.

To explore the SAR of the 6-aryl domain of the lead compound **15**, we first attempted to prepare the triflate of **109** using the procedure described for PMP analogue **108**. However triflation was not successful in this case, probably due to the presence of the pyridine moiety. We then explored the conditions developed by Kang and co-workers⁴² for the PyBroP-mediated activation of tautomerizable heterocycles. Treatment of **109** with PyBroP at room temperature for 2 hours resulted in the formation of the activated intermediate **113** as monitored by mass spectrometry that was not isolated, but directed coupled to phenylboronic acid under standard Suzuki conditions to afford the desired product in a respectable 74% yield (Scheme 3). Hydrolysis of the ethyl ester and HPLC purification provided lead compound **15** in 81% yield that possessed identical ¹H NMR, ¹³C NMR, HRMS data to the compound obtained from commercial vendor Enamine. The success of the Kang protocol for activation of **109** highlights the chemoselectivity of PyBroP-mediated activation for highly functionalized heterocycles.

We used parallel synthesis to prepare a systematic series of fifty-four (hetero)aryl-substituted analogues with substitution at C-6 (Scheme 3). Parallel synthesis was performed on a 0.33 millimole scale employing 100 mg of pyrazolopyridone **109** in 8 mL sealed vials using stock solution of all reagents. Extraction of the products from the reaction mixtures was achieved with dichloromethane using phase-separation cartridges. The esters were purified by flash chromatography with an average yield of 64% (range 7–97%), an excellent result considering that a standard purification method was utilized for all compounds. In some cases, when halogenated (hetero)arylboronic acids were used, more than one product was obtained due to a second Suzuki coupling (compounds **73**, **74** and **85**, tables 5 and 6). Whenever possible the two products were isolated. Hydrolysis of the esters was performed with NaOH in THF–H₂O with good yields affording compounds **15**, **37–59**, **61–62** and **66–90** (structures in Tables 5 and 6), which were purified by HPLC and lyophilized. The

PyBroP-activated intermediate **113** was also used to successfully introduce alkene groups using similar conditions to provide analogues **91** and **92** after ester hydrolysis (Scheme 3).

BOP-mediated coupling of the pyrazolopyridone **109** with three different amines was performed successfully using the procedure developed by Wan *et al.*,⁴³ further increasing the scope of this key intermediate and the range of substituents in the pyrazolopyridine at C-6 (Scheme 3). Analogues **95–97** were thus obtained following ester hydrolysis. Simple hydrolysis of the pyrazolopyridone intermediate **109** afforded analogue **98**, which lacks a 6-aryl moiety (Scheme 3).

A further series of C-6 substituted analogues was prepared as shown in Scheme 4. Analogue **60** incorporating salicylic acid at C-6 was prepared from **59-Ethyl ester** through simultaneous cleavage of the methyl ether and ethyl esters by treatment with boron trifluoride–dimethyl sulfate complex. We were also interested in evaluating the impact of increased lipophilicity of the lead compound **15**, hence a short series of analogues was synthesized bearing a 4-alkoxyphenyl group with 8, 12 and 16-carbon linear alkyl chains (compounds **63–65**). This strategy was successful in our previous SAR studies of Sal-AMS (**12**), maintaining or even increasing the respective inhibitory potency against MbtA, the AAAE from *M. tuberculosis*.⁴⁴ These compounds were synthesized through alkylation of **42-Ethyl ester** with the corresponding alkyl bromides (Scheme 4). The resulting esters were then hydrolyzed with NaOH to afford compounds **63–65**. We also prepared two alkyne analogues by PyBroP activation of **109** and subsequent palladium-catalyzed Sonogashira with triethylsilylacetylene and phenylacetylene under copper-free conditions employing PdCl₂(CH₃CN)₂ and Buchwald's 2-(dicyclohexylphosphino)biphenyl ligand to afford **114** and **115** (Scheme 4).⁴⁵ Notably, standard Sonogashira conditions did not afford any of the desired product. Deprotection of the terminal TES group in **114** with TBAF furnished **116**. Saponification of **115** and **116** with NaOH in aqueous THF provided **94** and **93**, respectively.

A small series of analogues was prepared as shown in Scheme 5 to study the modification at C-4 of the lead compound **15**. LiAlH₄ reduction of **18** provided hydroxy analogue **19**. A series of amides **22–25** and **27–28** was synthesized by conversion of **15** to the corresponding acid chloride employing oxalyl chloride followed by aminolysis. Functional group interconversion of carboxylic acid **15** to amine **21** was achieved by Curtius rearrangement of the respective acyl azide.

To explore the importance of the N-2 and N-7 atoms of the pyrazolo[3,4-*b*]pyridine scaffold we prepared analogues **16** and **17** from 6-bromo-1*H*-indazole-4-carboxylate **117** and 6-bromo-1*H*-indole-4-carboxylate **118** (Scheme 6). Alkylation of indazole **117** with 4-(bromomethyl)pyridine hydrobromide employing Cs₂CO₃ afforded a mixture of regioisomers **119** and **121** in 31 and 19% yield, respectively favoring the desired N-1 alkylated product. Indole **120** was prepared analogously from **118** in 77% yield. All three compounds were subjected to Suzuki coupling with phenylboronic acid and the methyl esters were hydrolyzed to provide the final compounds **16**, **17** and **99**.

Direct binding studies

The binding of all analogues to BasE was measured using a fluorescence polarization (FP) assay that measures displacement of the active-site directed fluorescent probe FI-Sal-AMS **14** (see Figure 3) from BasE, which results in an increase in polarization.³⁹ Fitting of the resultant displacement curve following the analysis described by Wagner and co-workers enables determination of the ligand dissociation constant.⁴⁶ We had previously demonstrated that our direct-binding FP assay agrees closely with results obtained by

isothermal titration calorimetry and a functional steady-state kinetic assay that measures acylation of the native aryl-carrier protein domain of BasF.³¹ Although this manuscript is primarily focused on *A. baumannii* and inhibition of BasE, we also evaluated all compounds against the homologue MbtA from *M. tuberculosis* as a means to assess inhibitor specificity toward other AAAEs. MbtA was selected since it is a representative AAAE that utilizes salicylic acid (SAL) instead of 2,3-dihydroxybenzoic acid (DHB) as the native aryl acid substrate.

Direct binding experiments were performed in a 96-well plate format in a 100 μ L volume containing 20 nM Fl-Sal-AMS **14** and 200 nM BasE or 50 nM MbtA. Fitting of the experimental data in the form of measured anisotropy (A_{OBS}) versus test compound concentration (L_{ST}) to equations 1 and 2 (see Experimental Section) provides the equilibrium dissociation constant (K_{D}) for each compound. The K_{D} of the lead compound **15**, previously determined as 78 nM against BasE from a purchased sample³⁹ was re-determined here as 36 nM for BasE and 3.7 μ M for MbtA for a newly synthesized and purified sample.

The importance of the 1*H*-pyrazolo[3,4-*b*]pyridine scaffold was evaluated with indazole **16** and indole **17** analogues wherein the N-2 and N-7 atoms are replaced with CH isosteres (Table 2). Deletion of N-7 in indazole **16** is well tolerated resulting in a 2-fold loss of potency toward BasE. By contrast, removal of N-2 in indole **17** results in a drastic 1400-fold loss of affinity toward BasE. A similar trend for **15–17** was observed for MbtA; however, the relative magnitudes difference in binding affinities were different. These results demonstrate that the pyrazole N-2 nitrogen atom is essential while the N-7 nitrogen atom is dispensable for potent activity.

Next, the role of the carboxylic acid at C-4 in **15** was assessed with a series of twelve analogues (Table 3). All modifications to the carboxylic acid lead to a decrease in binding affinity. Deletion of the carboxy group in **20** results in a complete loss of affinity while ethyl ester **18** is 60-fold less potent. Notably, the neutral carboxamide **22** and hydroxymethyl **19** are the best tolerated of all modification producing a modest 1.8- and 2.8-fold loss in affinities for BasE. In the amide series (compounds **23–28**), substitution of the amide provides a minor-to-modest decrease in potency toward BasE when compared to the carboxamide **22**, varying from 2.2- to 13.6-fold. However, no clear trend in regards to steric or electrostatic interactions is observed. Finally, replacement of the carboxy group with an amino group in **21** is surprisingly well tolerated for BasE resulting in an approximately 6-fold loss in potency. Collectively, these results suggest that a hydrogen-bond donor at C-4 is required (**18** and **20** vs. **19** and **21**), the electrostatic interaction of the negatively charged carboxylate is not important (**15** vs. **22**), and that small alkyl substituents are reasonably tolerated (**25–27**). Similar trends were observed with MbtA except that substituted amides were not accepted.

All modifications performed at N-1 lead to either complete loss in affinity or drastic loss of potency against both BasE and MbtA (Table 4). Even a minimal change, such as transposition of the pyridine ring nitrogen from the *para* to the *meta* position causes complete loss of affinity against both enzymes. The only compound in this series that maintains modest activity (a 15-fold decrease in affinity toward BasE and no activity against MbtA) is *p*-hydroxyphenylmethyl **32**, which possesses a hydrogen-bond acceptor moiety at an equivalent position as the 4-pyridyl substituent in **15**.

Extensive SAR studies were then carried out at C-6 of **15**, as it soon became evident that this was the most amenable to modification. Accordingly, sixty-two analogues were synthesized and the respective results are shown in table 5, for phenyl derivatives, and table 6, for other

analogues including heterocycles, amines, alkenes and alkynes. The results obtained in this series are quite promising, as there are sixteen compounds that improved or equaled the potency of the lead compound **15**, notably compounds **42**, **45**, **51**, **67** and **79**, with K_D 's under 10 nM toward BasE. The actual K_D values for these compounds may be even lower since these are already at the lower detection limit of the fluorescence polarization assay.

Thirty-eight analogues (**37–74**) were synthesized in the C-6 phenyl series (Table 5). Unless explicitly stated the SAR refers to BasE and the differences in activity are relative to lead compound **15**. A methyl, hydroxy and chloro scan of the *ortho*-, *meta*-, and *para*-positions was performed (compounds **37–42**, **44–46**) to assess the ability to tolerate substitution at each position. All substitutions at the *ortho* position result in a decrease in affinity ranging from 7- to nearly 70-fold. Both *o*-methyl **37** and *o*-chloro **44** possess a drastic loss in affinity (60- to 70-fold), whereas the *o*-hydroxy **40** is only 7-fold less potent, perhaps due to a possible intramolecular H-bond formed with the adjacent pyridine nitrogen, which could stabilize the structure in a favorable conformation. Substitution at both the *meta*- and *para*-positions is better tolerated. While most compounds result in a modest decrease in affinity ranging from 3- to 6- fold, *m*-chloro **45** and *p*-hydroxy **42** are more than 4-fold more potent than **15**. The observed SAR with respect to MbtA has a nearly identical trend except that *p*-methyl **39** is the most potent toward MbtA with a 2.6-fold increase in affinity.

Based on the ability to tolerate substitution at the *para*-position, we prepared a systematic series of seventeen analogues with a range of functional groups (**43**, **47–62**). Among this initial series *p*-nitro **51** is the only analogue with substantially improved potency resulting in a 9-fold increase in affinity. Several other analogues including *p*-fluoro **48**, *p*-bromo **47**, *p*-methylthio **61**, *p*-cyano **56**, and *p*-methylsulfonyl **55** possess a modest increase in affinity ranging from 1.3- to 2.8 fold. However, the majority of analogues are less potent resulting in a modest decrease in affinity from 2.2-fold for *p*-amino **52** and *p*-methoxy **62** to over 20-fold for *p*-acetylamino **54** and *p*-carboxylate **58**. The combination of a *para*-carboxylate and a *meta*-hydroxy in salicylate **60** is only 4.7-fold less potent, showing that the additional *meta*-hydroxy is able to partially restore binding affinity. Overall, no clear trends emerged in regards to steric or electronic effects. The SAR of this series with respect to MbtA does not parallel that observed for BasE with *p*-methylsulfonyl **55** displaying the highest affinity (29-fold greater than **15**) and *p*-carboxy **58** the lowest affinity (2-fold lower than **15**) among the *para*-substituted analogues.

We next explored bulky hydrophobic groups (**63–74**) to define a steric boundary of the active-site (Table 5). Long chain alkoxy groups (compounds **63–65**) reduce binding affinity and result in poor solubility (compound **65** was insoluble in the assay conditions). Since the bulky phenyl group in *p*-phenoxy **66** does not adversely affect affinity, we decided to further explore the SAR with other groups and synthesized *p*-biphenyl **72** that is 3.5-less potent and *p*-benzoyl **70**, which is 2-fold more potent. Introduction of a CH₂ spacer in *p*-phenoxy **66** provided *p*-benzyloxy **67** that possesses an impressive 17-fold increase in affinity. Further addition of a *p*-methoxy group to **67** affords 4-methoxybenzyloxy **68** that is a 21-fold less potent than **67**. The overall SAR trends for this series of compounds with respect to MbtA do not correlate very closely with BasE. *p*-Benzoyl **70** is the most potent analogue of MbtA with a K_D of 19 nM, which is an astonishing 197-fold more potent than the lead compound **15**. Among the series of compounds in Table 5, *p*-benzyloxy **67** and *p*-benzoyl **70** emerged as the most attractive due to their high affinities toward BasE. Additionally, **70** was deemed particularly interesting as a result of its balanced activity against both MbtA and BasE.

We also synthesized a series of 24 analogues **75–98** containing a wide variety of heterocycles, alkenes, alkynes and amines at C-6 (Table 6). The 5-membered furan and thiophene heterocycles were initially examined with analogues **75–76** and these are nearly

10-fold less potent than **15**. A methyl scan in the thiophene ring with compounds **77–79** showed that substitution at positions 3 and 4 (**77–78**) is not well tolerated resulting in a respective 9- and 2.4-fold decrease in affinity; however, a 5-fold increase in affinity is conspicuously observed at position 5 (compound **79**). Given the enhanced affinity of 5-methyl substituted thiophen-2-yl group, we also evaluated benzothiophene **80**, 5-(acetyl)thiophene **81**, and 5-(chloro)thiophene **82**, but none of these enhance affinity. All of the nitrogen-containing heterocyclic analogues including pyridines **83–84**, bipyridine **85**, isoquinoline **86**, indole **87**, quinoline **88**, pyrimidine **89** and pyrazole **90** result in a loss of potency ranging from 1.7-fold for indole **87** to 215-fold for isoquinoline **86**. Similarly, alkene and alkyne analogues **91–94** bind with lower affinities ranging from ~10-fold for phenylethenyl **92** and phenylethynyl **94** to ~55-fold for unsubstituted analogues ethenyl **91** and ethynyl **93**. Amino analogues including benzylamine **95**, morpholine **96** and 3-hydroxypropylamine **97** are 40-fold to 68-fold less potent. Analogue **98** lacking an aryl moiety at C-6 is completely inactive (> 2800-fold less potent). Collectively, the results from this series of analogues demonstrate that a phenyl or isosteric heterocycle is required at C-6 (**91**, **93**, **95–98**) and nonpolar heterocycles are optimally tolerated (**79**, **80**, **82** vs. **89** and **90**). Overall, no improvement in affinity was achieved for **75–98** with BasE. The SAR of this series for MbtA is markedly different and several compounds were identified that are more potent including benzothiophene **80**, 5-(acetyl)thiophene **81**, 5-(chloro)thiophene **82**, 6-chloropyridine **84**, and bipyridine **85**, which possess 12-, 5-, 14-, 4-, and 10-fold higher affinities relative to **15**.

To complete our cursory SAR studies of **15**, we also evaluated two compounds prepared during the course of our studies that involve double modifications (Table 7). Compound **99** containing an indazole core, but with the (4-pyridyl)methyl group at position 2 instead of 3, retains some potency toward MbtA (15.5-fold loss) and a pronounced 1800-fold loss in affinity toward BasE. Compound **100** with two unfavorable modifications (replacement of the 1-(4-pyridyl)methyl group and introduction of an amino group at position 6) displays no affinity toward either BasE or MbtA.

Structural Characterization of Inhibitors with BasE

The active site of BasE, like all AAAE enzymes, contains three subsites that are used to bind the nucleotide, the aromatic acid, and the pantetheine chain of the incoming carrier protein that is used in the thioesterification reaction.³⁴ The binding pocket for the nucleotide base is bordered on one side by a conserved aromatic residue and on the other by main chain interactions. The aromatic acid binds in a well-defined pocket of the AAAE.⁴⁷ Finally, the pantetheine moiety of the cofactor enters the active site through a long tunnel formed between the larger N- and smaller C-terminal domain of the adenylyating enzyme. This tunnel forms in the related acyl-CoA synthetases through rotation of the C-terminal domain upon completion of the initial adenylation reaction to form a conformation that is competent for thioester-formation.³¹

We have previously reported on the crystal structure of BasE bound to DHB-AMS **13**, a derivative of **13** bearing an aliphatic chain on the C-2 position of the adenine, and the parent compound **15**.³¹ The structure of BasE bound to **15** shows that the pyridine approximates the binding mode of the DHB substrate. The nitrogen of the pyridine moiety hydrogen bonds to the side chain of Asn242, mimicking the binding interaction of the 2- and 3-hydroxy groups of DHB in the structure of BasE bound to **13**.³¹ Unexpectedly, the binding of **15** did not utilize the carboxylate to mimic the adenylate phosphate nor occupy the adenine binding pocket. The phenyl moiety was placed into the pantetheine tunnel. The binding of the phenyl group in this tunnel provides room for the larger inhibitors that were observed to result in

higher affinity for BasE. We therefore determined the crystal structure of BasE bound to **67** and **70**, to examine how the larger aromatic substituent would fill the pantetheine tunnel.

Crystals of BasE complexes with compounds **67** and **70** diffract well, and the structures were determined by difference Fourier methods. Data collection and refinement statistics are presented in Table 8. As with the previous structures of BasE³¹ and other ANL adenylating enzymes,^{48, 49} the conformationally dynamic C-terminal domain is disordered and is not included in the final models.

The two ligands bind in the active site of BasE in a manner identical to that of **15** reported previously.³¹ The pyridin-4-yl-methyl group enters into the DHB binding pocket, forming a hydrogen bond with the side chain of Asn242. This interaction is important for binding, as seen in compounds **29** through **36** (Table 4) where only compound **32** retained some binding affinity. SAR of the core heterocycle (Table 2) demonstrates the importance of N-2 of the pyrazole ring. The N-2 of the pyrazole ring accepts a hydrogen bond from the main chain amine of Gly338. Loss of this interaction results in a reduction of affinity of three orders of magnitude. This interaction is unique to the HTS ligands as the amide of Gly338 does not interact with the DHB-AMS analog of the adenylate **13**. In contrast, the N-7 nitrogen of the pyrazolopyridine makes no interactions with the BasE active site residues and therefore substitution with a carbon has relatively little impact on binding. The carboxylate groups of **67** and **70** interact with the side chain of Arg435. The interaction of compound **67** with Arg435 is different from that of compounds **15** and **70**. However we note that the electron density for this residue, which is only 2 residues from the hinge that separates the N-terminal domain from the disordered C-terminal domain, is disordered in one chain in the asymmetric unit for each protein model, therefore it is likely that Arg435 adopts multiple conformations. Nevertheless, the density is of sufficient quality to be modeled in the second chain in the asymmetric unit for each complex. In the structure of BasE bound to **70**, the side chain of Arg435 appears to make a bivalent interaction with the carboxylate. In the model for BasE bound to **67**, the side chain of Arg435 interacts with just a single oxygen from the carboxylate. Furthermore, in the previously reported complex with **15**, the side chain of Arg435 does not interact directly with the carboxylate of this compound, rather this is mediated through a water molecule. This fact further strengthens our hypothesis of multiple conformations adopted by this residue, and could also justify the higher affinity to BasE observed for compounds **67** and **70** (direct interaction between Arg435 and the carboxylate) when compared to **15**. SAR with compounds altered in this carboxylate (**18** through **28**, Table 3) illustrates a complicated relationship of this group to binding affinity. Replacement of the carboxylate with an alcohol or a carboxamide are reasonably well tolerated in compounds **19** and **22**, resulting in only a 3- and 2-fold increase in K_D . This shows that a strict ionic interaction is not required with the side chain of Arg435.

The longer hydrophobic moieties present in **67** and **70** continue into the pantetheine tunnel (Figure 5). The phenyl ring shared by **15**, **67**, and **70** stacks against the side chain of His241. The benzyloxy group of **67** and the benzoyl ring of **70** adopt different conformations. The ring in **67** is positioned closer to the pocket formed by Pro266, Val286, and Ala 289 whereas the ring of **70** is positioned near the top of the groove near residues Leu109 and Pro238. The binding of the phenyl group into this hydrophobic pocket helps to explain the affect of changes at the *ortho*-position in compounds **37** and **44**. The ring is 4.1–4.3 Å from the side chain of Phe243 on one side. The *ortho*-carbon on the other side points toward the location of the disordered C-terminal domain and we cannot determine if it could be accommodated here. The phenyl ring and the pyrazolopyridine core are nearly coplanar, with inter-planar torsion angles ranging from 3° to 15° in the three inhibitor molecules, and the *o*-hydroxy analog **40** may be tolerated because the hydroxyl could hydrogen bond with the adjacent N-7 nitrogen from the pyrazolopyridine core.

Interestingly, whereas **70** serves as a potent inhibitor for both BasE and MbtA, **67** serves as a nanomolar inhibitor for BasE, but is 1000-fold weaker with MbtA (Table 5). Examination of the binding pockets of the two inhibitor complex and a sequence alignment of BasE and MbtA shows that the residues labeled in Figure 5 are conserved between BasE and MbtA, with the exception of Pro238 and Ala289, which are replaced by alanine and leucine, respectively, in MbtA. The replacement of Ala289 with the bulkier leucine is likely the reason why **67** is unable to bind in the same manner as observed in the BasE crystal structure, resulting in the observed micromolar binding constant. We note, however, that the disordered C-terminal domain does form a portion of the pantetheine tunnel in which the aromatic groups bind. Therefore, together with the differences in residues between BasE and MbtA, the C-terminus may also contribute to binding of the inhibitors and be responsible for the different binding affinities observed.

Antibacterial activity

All of the final compounds **15–100** were evaluated for antibacterial activity against *A. baumannii* ATCC 19606 under iron-deficient (1 μ M FeCl₃ and 200 μ M dipyriddy as chelating agent) and iron-replete conditions (200 μ M FeCl₃) by broth microdilution in M9 minimal media supplemented with casamino acids (see Experimental Section). However, none of the compounds exhibited antibacterial activity against this bacterium. Several ester intermediates of the most potent inhibitors were also tested to assess whether the higher lipophilicity of these could lead to improved uptake by the bacterium, assuming that a bacterial esterase would hydrolyze the esters. Again, no activity was observed for the esters tested. The resistance of *A. baumannii* to many antibiotics is caused by numerous mechanisms including multidrug efflux pumps and permeability defects due to loss of porins.⁵⁰ This could explain the resistance to **15** and its analogues, but further studies are required to assess this hypothesis. A small selection of compounds that exhibited potent activity toward MbtA, namely **15**, **18**, **66**, **70**, and **82** and their ethyl esters were also tested against *M. tuberculosis* H37Rv, under iron-deficient and iron-replete conditions (Table 9). While some of these compounds displayed very modest activity, the activity under iron replete conditions suggests these compounds may operate by a secondary mechanism of action since siderophore synthesis in *M. tuberculosis* is dispensable under rich-conditions.²²

Disruption of BasE in *A. baumannii*

Earlier studies had rigorously demonstrated the importance of acinetobactin production for growth under iron limiting conditions by insertional inactivation of BasD, the cyclase-condensation domain NRPS involved in acinetobactin biosynthesis.^{27, 28} Based on our inability to obtain antibacterial activity against *A. baumannii* ATCC 19606, we hypothesized that BasE may be functionally redundant, although no other AAAE's are present in the genome. In order to unequivocally demonstrate the role of BasE in acinetobactin biosynthesis, we deleted *basE* by homologous recombination replacing it with a kanamycin resistance gene on the chromosome. The deletion was confirmed by PCR (data not shown). Under iron deficient conditions,²⁷ the mutant was severely impaired for growth (Figure 6A). However, under iron-replete conditions,²⁷ there was little observable difference between the growth rates between the wild-type and mutant knockout strain, except for a slight increase in lag-time for entry in exponential growth (Figure 6B). The modest growth observed for the *basE* mutant in Figure 6A under iron deficient conditions is caused by residual bacterial iron stores present in the initial inoculum. If the strain is pre-conditioned under iron-deficient conditions and then inoculated into iron deficient media, it is unable to grow. Reintroduction of *basE* on a plasmid was able to partially complement the deletion phenotype (Figure 6A). The inability to fully complement the *basE* knockout strain may be caused by a polar effect on the downstream pathway. The gene immediately downstream of *basE*, *basF* may be transcriptionally coupled to its upstream neighbor as there are only 18 bp between the two

genes and there is no easily recognizable Shine-Dalgarno sequence in this region. Attempts to remove the kanamycin resistance gene and create a clean deletion of *basE* were unsuccessful. In summary, these results in conjunction with prior genetic studies on acinetobactin synthesis suggest BasE is nonredundant and required for growth of *A. baumannii* under iron-restricted conditions with inorganic iron as the sole source of iron.

Discussion

The importance of iron for bacterial pathogenesis has led to an increasing interest in targeting iron acquisition pathways for antibacterial development.^{51–53} The most ubiquitous strategy employed by bacteria to obtain iron is the synthesis of siderophores.¹² Many bacteria also possess a heme uptake pathway, but this is only important to support bacteremia or bloodstream infections.⁵⁴ However, inhibition of siderophore biosynthesis is unlikely to provide broad spectrum antibiotics due to large number of structurally different siderophores produced by bacteria.⁵⁵ Given the alarming rise of antibacterial resistance and the extreme challenges of developing new classes of broad-spectrum agents, the synthesis of narrow spectrum antibiotics is becoming more attractive, particularly for serious infections like *A. baumannii* for which there are few other treatment options.⁵⁶

Collins and co-workers have shown that bactericidal antibiotics generate hydroxyl radicals through the Fenton reaction caused by release of Fe²⁺ from bacterial iron-sulfur proteins.^{23, 24} We hypothesize that siderophores may protect bacteria from ROS by chelating free iron. A recent study demonstrated that enterobactin (the prototypical aryl-capped siderophore from *E. coli*) protected this bacteria from oxidative stress.⁵⁷ Thus, inhibition of siderophore biosynthesis may have the additional benefit of enhancing the bactericidal activity of existing antibiotics.

Quadri and co-workers were the first to report an inhibitor of siderophore biosynthesis with the synthesis of Sal-AMS, the prototypical AAAE inhibitor.^{35–37} Unfortunately, Sal-AMS and related nucleoside analogues have only limited activity against Gram-negative pathogens. We believe this is a result of their highly polar nature and formal negative charge that likely prevents uptake across the negatively charged outer lipopolysaccharide-rich membrane of Gram-negative organisms. The confirmed role of aryl-capped siderophores for virulence in Gram-negative infection including acinetobactin, enterobactin, and yersiniabactin, coupled with lack of activity of Sal-AMS toward *A. baumannii*, *K. pneumoniae*, *P. aeruginosa*, and *E. coli* motivated us to search for alternate scaffolds as AAAE inhibitors.

We identified pyrazolopyridine **15** using a high-throughput fluorescence polarization assay with BasE from *A. baumannii* and performed detailed SAR studies.³⁹ The N-2 nitrogen atom of the pyrazolopyridine scaffold **15** is essential while the N-7 nitrogen is not required for potent activity. Analysis of the co-crystal structures of **15**, **67**, and **70** show a hydrogen bond between N-2 of the pyrazolopyridine and the amide NH of Gly338 whereas no interaction is observed with N-7. The pyridylmethyl substituent at N-1 is optimal and binds in the DHB pocket with the pyridine substituent occupying a position nearly identical to the native DHB ligand forming a hydrogen bond to Asn242. The importance of this hydrogen bond was assessed by isosteric replacement of the pyridine N with a CH, which resulted in a greater than 2800-fold decrease in binding affinity that corresponds to a staggering loss of more than 4.8 kcal/mol in binding energy. The carboxylate substituent at C-4 is preferred, but can be replaced by neutral isosteres such as a carboxamido or hydroxymethyl with only a modest 2–3-fold attenuation in potency. Presumably these analogues can maintain the interaction with Arg435 observed with **15**, **67**, and **70**. The phenyl substituent at C-6 is the most tolerant to modification and resulted in the identification of *p*-hydroxyphenyl **42**, *p*-

nitro **51**, *p*-methylsulfonylphenyl **55**, *p*-benzyloxyphenyl **67** and *p*-benzophenone **70**, which are up to 18-fold more potent than **15**. Analysis of the co-crystal structures of **67** and **70** reveals that the larger *para*-substituents are accommodated in the pantetheine tunnel. Thus, the pyrazolopyridine analogues are considered multisubstrate inhibitors since they occupy the binding sites of all three BasE substrates (DHB, ATP, and pantetheine cofactor of BasF).

MbtA was also studied as a representative salicylate adenylating enzyme, which are found in *M. tuberculosis*, *Yersinia* sp. and *K. pneumoniae*. The lead compound **15** and its analogues are generally more active against BasE than MbtA. Benzophenone **70** is the most potent inhibitor of MbtA with a K_D of 19 nM, a value approximately 200-fold lower than the lead compound **15**. Moreover, **70** is equipotent against both MbtA and BasE demonstrating the feasibility of identifying an inhibitor with balanced activity despite differences in the active-site architecture between these enzymes.

Surprisingly, in spite of the low nanomolar dissociation constants of some of the BasE inhibitors in the biochemical assay, they failed to inhibit growth of *A. baumannii* in vitro. A selection of compounds was also tested against *M. tuberculosis* that encodes for MbtA, a homologue of BasE. Modest bacteriostatic activity was observed with MICs varying between 25 and 100 μ M. However the MICs were identical under iron-deficient and iron-replete conditions indicating that inhibition of MbtA is not fully responsible for the observed activity. Further work will be necessary in order to improve and verify the ability of this series of compounds to penetrate *A. baumannii* and reach their enzyme target BasE as discussed above.

The structure for acinetobactin was described in 1994 as **11** (Figure 2).²⁵ In 2008 Walsh and Sattely revised the structure of acinetobactin to **1** based on their astute observation of the structural dissimilarities of pseudomonine and acinetobactin despite a common organization of their respective biosynthetic gene clusters.^{29, 30} The iron-binding properties of acinetobactin have not been evaluated, but it is expected to possess a substantially lower affinity for Fe^{3+} than pre-acinetobactin, which contains an oxazoline and hydroxamate functions. In acinetobactin these functional groups rapidly rearrange ($t_{1/2} \sim 1$ hour) to provide the isoxazolidinone in **1** (Figure 2). The revised structure **1** has been confirmed via total synthesis.²⁶

The importance of acinetobactin for iron acquisition was first studied in *A. baumannii* strain ATCC 19606.^{27, 28, 58} Insertional inactivation of *basD*, which encodes for a didomain protein responsible for the condensation of the DHB and L-Thr building blocks in acinetobactin biosynthesis, results in a strain incapable of producing acinetobactin.²⁸ The *basD* knockout is impaired in the ability to replicate under iron deficient conditions,²⁷ in human A549 alveolar epithelial cells,⁵⁹ and in a mouse sepsis model.⁶⁰ While these studies clearly demonstrate the importance of *basD* for virulence, we wished to confirm that *basE* also phenocopies the *basD* mutant since these isogenic mutants will potentially produce different siderophore intermediates that may partially rescue loss of acinetobactin. In this study we examined the importance of *basE* for virulence of *A. baumannii* strain ATCC 19606. Deletion of *basE* results in a strain unable to replicate under iron deficient conditions, but that grows at the same rate as the wildtype strain under iron-replete conditions. These results confirm BasE as a valid target and suggest the inability of the pyrazolopyridine inhibitors to exhibit whole-cell activity toward *A. baumannii* is due to other factors such as limited accumulation and/or lack of vulnerability of BasE to inhibition by small-molecules. Vulnerability or amount that a target must be inhibited is another important consideration that cannot be assessed by a simple knockout strain.

The initial studies of iron acquisition in *A. baumannii* focused on strain ATCC 19606 and demonstrated acinetobactin is the only siderophore produced by this organism.²⁵ Genome sequencing of the related strain *A. baumannii* ATCC 17978, reveals it encodes for an additional siderophore pathway of an uncharacterized aryl-capped siderophore.¹⁶ As a result acinetobactin is dispensable in ATCC 17978.¹⁶ Analysis of the second siderophore gene cluster reveals it encodes for two 2,3-dihydroxybenzoate-AMP ligases (A1S_2573 and A1S_2574), which we expect can also be inhibited by our pyrazolopyridine BasE inhibitors.^{59, 61, 62} Comparative genomics studies of six fully sequenced *A. baumannii* strains and PCR analysis of 50 clinical isolates were recently described providing the most detailed picture yet reported of iron acquisition systems in this pathogen.⁶² The acinetobactin gene cluster is highly conserved among clinical isolates. Another prevalent gene cluster was identified, which encodes for a putative hydroxamate siderophore. Genes encoding for ferrous uptake and heme uptake are also observed in virtually all strains. The importance of these multiple iron acquisition systems for virulence remains to be evaluated, but suggests this pathogen is capable of using alternate iron sources for survival under different environmental conditions.

Conclusion

A comprehensive analysis of the structure–activity relationships of the HTS hit **15** was performed that examined the importance of the pyrazolopyridine heterocycle, the 4-pyridylmethyl substituent at N-1, the carboxylic acid at C-4, and the phenyl group at C-6 for binding to BasE and MbtA. BasE from *A. baumannii* was the primary focus of the work and the initial SAR studies defined the crucial interactions necessary to maintain potency and also identified sites amenable to modification. The pyrazolopyridine heterocycle ideally positions the N-1, C-4, and C-6 substituents into the DHB, ATP, and pantetheine binding pockets. The N-2 nitrogen of the pyrazolopyridine forms a key hydrogen bond with the amide backbone of Gly338, but N-7 is dispensable for potent activity. The pyridylmethyl substituent at N-1 is crucial illustrated by the almost 5 kcal/mol loss in binding affinity by simple deletion of the nitrogen atom in the pyridine. The carboxylic acid at C-4 is not required and can be replaced with alternate hydrogen-bond acceptor moieties including hydroxymethyl and carboxamido with only a modest attenuation in binding affinity demonstrating the ionic interaction observed between the carboxylic acid and Arg435 in the co-crystal structures of BasE with three different pyrazolopyridine ligands is not critical. The C-6 phenyl group is most tolerant to substitution and hydrophobic (hetero)aryl substituents are preferred. *p*-Benzyloxyphenyl **67** was identified as the most potent analogue toward BasE with a K_D of 2 nM. The entire compound series was also evaluated against MbtA, a representative AAAE that activates salicylic acid and similar SAR trends were observed. HTS hit **15** is considerably less potent toward MbtA with K_D of only 3.7 μ M. However, benzophenone **70** was found to have balanced activity against both BasE and MbtA with a K_D of 19 nM, which represents a nearly 200-fold increase in potency toward MbtA. The SAR and structural characterization of ligands with BasE described herein provide a foundation for future studies to improve upon the antibacterial activity and exploit the unique multisubstrate modality of inhibition.

Experimental Section

Chemistry: General Methods and Materials

All commercial reagents (Sigma-Aldrich, Acros, Alfa-Aesar) were used as provided. Boronic acids and boronic acid pinacolate esters were purchased from Aldrich, Boron Molecular (Research Triangle, NC), and Frontier Scientific (Logan, UT). Compounds **20**, **26**, **29–30** and **33–35** were purchased from Enamine (Ukraine). Compounds **117** and **118** were obtained from Sinova (Bethesda, MD). Compounds **104**,⁶³ **114**,⁴⁵ and **115**⁴⁵ were

prepared according to the respective literature procedure. Purity (95%) of all final compounds was confirmed by reverse-phase HPLC using the indicated method (see Supporting Information). An anhydrous solvent dispensing system (JC Meyer, Laguna Beach, CA) using 2 packed columns of neutral alumina was used for drying THF, DMF and CH₂Cl₂ and the solvents were dispensed under argon. All reactions were performed under an inert atmosphere of dry Ar or N₂ in oven-dried (150 °C) glassware. Flash chromatography was performed with an ISCO Combiflash Companion® purification system with prepacked silica gel cartridges supplied by Luknova, with the indicated solvent system. Preparative HPLC was performed on a Varian Microsorb MV 100-8 C18 column (41.4 × 250 mm, 8 μm particle size) operating at 40 mL/min with detection at 254 nm in the conditions described in the Supporting Information. ¹H and ¹³C NMR spectra were recorded on either Varian 600 MHz or Bruker Avance 400 MHz spectrometers. Proton chemical shifts are reported in ppm from an internal standard of residual chloroform (7.26 ppm), dimethylsulfoxide (2.50 ppm) or methanol (3.31 ppm), and carbon chemical shifts are reported using an internal standard of residual chloroform (77.1 ppm), dimethylsulfoxide (39.5 ppm) or methanol (49.0 ppm). Proton chemical data are reported as follows: chemical shift, multiplicity (s = singlet, d = doublet, t = triplet, q = quartet, p = pentet, m = multiplet, br = broad, ovlp = overlapping), coupling constant, and integration. High-resolution mass spectra were obtained on an Agilent TOF II TOF/MS instrument equipped with an ESI interface.

Compounds from Scheme 1

Diethyl 2-(5-amino-1-(4-methoxybenzyl)-1H-pyrazol-4-yl)-2-hydroxysuccinate (106): A solution of diethyl oxalacetate (3.46 g, 18.4 mmol, 1.01 equiv) and **104**⁶³ (3.7 g, 18.2 mmol, 1.0 equiv) in benzene (40 mL) was heated at 65 °C for 20 h. The mixture was concentrated and purification by flash chromatography (3:2 hexanes/EtOAc) afforded the title compound (4.5 g, 63%) as a yellow oil: *R*_f 0.65 (EtOAc); ¹H NMR (600 MHz, CDCl₃) δ 1.23–1.27 (m, 6H), 2.92 (d, *J* = 16.8 Hz, 1H), 3.32 (d, *J* = 16.8 Hz, 1H), 3.78 (s, 3H), 4.08 (br s, 2H, NH₂), 4.16 (q, *J* = 7.2 Hz, 2H), 4.24 (q, *J* = 7.2 Hz, 2H), 5.06 (s, 2H), 6.85 (d, *J* = 8.4 Hz, 2H), 7.10 (d, *J* = 8.4 Hz, 2H), 7.23 (s, 1H); ¹³C NMR (150 MHz, CDCl₃) δ 14.17, 14.23, 43.9, 51.5, 55.4, 61.2, 62.4, 73.3, 102.7, 114.5, 128.1, 128.5, 135.8, 143.3, 159.4, 171.3, 173.5; HRMS (ESI⁺) calcd for C₁₉H₂₆N₃O₆ [M + H]⁺ 392.1816, found 392.1825 (error 2.3 ppm).

Ethyl 1-(4-methoxybenzyl)-6-oxo-6,7-dihydro-1H-pyrazolo[3,4-*b*]pyridine-4-carboxylate (108): A suspension of **106** (5.2 g, 13.2 mmol) in glacial acetic acid (40 mL) was refluxed for 3 h. The mixture was concentrated to approximately half of the volume, then isopropanol (100 mL) was added and the solution was cooled to room temperature. The product crystallized as a white solid (3.5 g, 81%): mp 235–236 °C; *R*_f 0.65 (1:1 EtOAc/hexane); ¹H NMR (600 MHz, DMSO-*d*₆) δ 1.37 (t, *J* = 7.2 Hz, 3H), 3.70 (s, 3H), 4.40 (q, *J* = 7.2 Hz, 2H), 5.46 (s, 2H), 6.86 (d, *J* = 8.4 Hz, 2H), 6.95 (br s, 1H), 7.16 (d, *J* = 8.4 Hz, 2H), 8.11 (s, 1H), 12.05 (br s, D₂O-exchangeable, 1H); ¹³C NMR (150 MHz, DMSO-*d*₆) δ 14.0, 49.5, 55.1, 61.7, 113.9, 128.7, 129.1, 133.0, 134.0, 158.7, 163.5, 164.2 (unable to observe 3 carbons—estimated at 99, 135, and 147 ppm due to quadrupolar coupling with nitrogen); HRMS (ESI⁺) calcd for C₁₉H₂₆N₃O₆ [M + H]⁺ 328.1292, found 328.1303 (error 3.4 ppm).

1-(Pyridin-4-ylmethyl)-1H-pyrazol-5-amine (105): To a solution of acrylonitrile (4.42 g, 83 mmol, 1.05 equiv) at 0 °C in absolute EtOH (80 mL), hydrazine hydrate (3.93 g, 79 mmol, 1.0 equiv) was added dropwise with vigorous stirring over 10 min. The ice bath was removed and the reaction was stirred for 24 h at rt. The reaction mixture was cooled to 0 °C and 4-pyridinecarboxaldehyde (8.8 g, 82 mmol, 1.04 equiv) was slowly added and stirring continued for 2 h at rt. The mixture was concentrated, the residue was dissolved in dry *n*-

butanol (30 mL) and a 16% sodium *n*-butoxide solution in *n*-butanol (100 mL, 167 mmol, 2.1 equiv) was added. The resulting solution was refluxed for 1 h, cooled to rt, and concentrated. The residue was partitioned between H₂O (150 mL) and EtOAc (3 × 150 mL). The combined organic layers were dried (MgSO₄) and concentrated to afford the title compound (10.6 g, 76%) as a pale brown solid: *R*_f 0.19 (9:1 EtOAc/MeOH); ¹H NMR (600 MHz, CDCl₃) δ 3.43 (br s, 2H, NH₂), 5.20 (s, 2H), 5.63 (d, *J* = 1.8 Hz, 1 H), 7.00 (d, *J* = 6.0 Hz, 2H), 7.35 (d, *J* = 1.8 Hz, 1H), 8.54 (d, *J* = 6.0 Hz, 2H); ¹³C NMR (150 MHz, CDCl₃) δ 50.3, 92.8, 121.7, 139.5, 144.6, 146.0, 150.4; HRMS (ESI+) calcd for C₉H₁₁N₄ [M + H]⁺ 175.0978, found 175.0976 (error 1.1 ppm).

Diethyl 2-(5-amino-1-(pyridin-4-ylmethyl)-1H-pyrazol-4-yl)-2-hydroxysuccinate (107):

A solution of diethyl oxalacetate (10.6 g, 56.1 mmol, 1.2 equiv) and **105** (8.1 g, 46.7 mmol, 1.0 equiv) in benzene (100 mL) was heated at 65 °C for 15 h. The mixture was concentrated and the residue was recrystallized from EtOH/Et₂O to afford the title compound (10.6 g 48%) as a pale yellow solid: mp 118–120 °C; *R*_f 0.61 (7:3 EtOAc/MeOH); ¹H NMR (600 MHz, CDCl₃) δ 1.27 (ovlp t, *J* = 7.2 Hz, 3H), 1.28 (ovlp t, *J* = 7.2 Hz, 3H), 2.95 (d, *J* = 16.8 Hz, 1H), 3.35 (d, *J* = 16.8 Hz, 1H), 4.16 (br s, 2H, NH₂), 4.19 (q, *J* = 7.2 Hz, 2H), 4.26 (q, *J* = 7.2 Hz, 2H), 5.13 (s, 2H), 7.01 (d, *J* = 6.0 Hz, 2H), 7.29 (s, 1H), 8.55 (d, *J* = 6.0 Hz, 2H); ¹³C NMR (150 MHz, CDCl₃) δ 14.20, 14.25, 43.9, 50.4, 61.3, 62.5, 73.3, 103.2, 121.8, 136.8, 143.6, 145.5, 150.4, 171.3, 173.4; HRMS (ESI+) calcd for C₁₇H₂₃N₄O₅ [M + H]⁺ 363.1663, found 363.1668 (error 1.4 ppm).

Ethyl 6-oxo-1-(pyridin-4-ylmethyl)-6,7-dihydro-1H-pyrazolo[3,4-*b*]pyridine-4-carboxylate (109):

A suspension of **107** (9.7 g, 26.9 mmol) in glacial acetic acid (60 mL) was refluxed for 4 h. The mixture was concentrated and the residue was triturated with isopropanol (100 mL). The white solid that formed was filtered, washed with isopropanol/ether and dried under vacuum to afford the title compound (6.29 g, 78%) as an off-white solid: *R*_f 0.25 (9:1 EtOAc/MeOH); ¹H NMR (600 MHz, DMSO-*d*₆) δ 1.39 (t, *J* = 7.2 Hz, 3H), 4.42 (q, *J* = 7.2 Hz, 2H), 5.61 (s, 2H), 7.00 (br s, 1H), 7.07 (d, *J* = 6.0 Hz, 2H), 8.20 (s, 1H), 8.49 (d, *J* = 6.0 Hz, 2H), 12.10 (br s, 1H); ¹³C NMR (150 MHz, DMSO-*d*₆) δ 14.0, 49.0, 61.7, 106.4, 109.0, 121.8, 133.6, 134.1, 146.1, 149.8, 163.8, 164.1 (missing 1 C); HRMS (ESI+) calcd for C₁₅H₁₅N₄O₃ [M + H]⁺ 299.1139, found 299.1128 (error 3.7 ppm).

Compounds from Scheme 2

Ethyl 1-(4-methoxybenzyl)-6-(trifluoromethylsulfonyloxy)-1H-pyrazolo[3,4-*b*]pyridine-4-carboxylate (110):

To a solution of **108** (3.38 g, 10.3 mmol, 1.0 equiv) and 2,6-di-*tert*-butyl-4-methylpyridine (3.18 g, 15.5 mmol, 1.5 equiv) in CH₂Cl₂ (50 mL) at –78 °C, was added dropwise a solution of trifluoromethanesulfonic anhydride (2.98 mL, 17.7 mmol, 1.7 equiv) in CH₂Cl₂ (10 mL). The reaction mixture was stirred at 0 °C for 4 h. The solvent volume was reduced to one-third *in vacuo* and diluted with EtOAc (40 mL). The resulting solution was washed consecutively with saturated aqueous NaHCO₃ (3 × 20 mL), H₂O (20 mL), 1 M aqueous HCl (3 × 20 mL), H₂O (20 mL) and saturated aqueous NaCl (20 mL). The organic layer was dried (MgSO₄) and concentrated. Purification by flash chromatography (4:1 hexane/EtOAc) afforded the title compound (3.2 g, 68%) as a white solid: *R*_f 0.43 (4:1 hexane/EtOAc); ¹H NMR (600 MHz, CDCl₃) δ 1.48 (t, *J* = 7.2 Hz, 3H), 3.76 (s, 3H), 4.52 (q, *J* = 7.2 Hz, 2H), 5.59 (s, 2H), 6.84 (d, *J* = 8.4 Hz, 2H), 7.37 (d, *J* = 8.4 Hz, 2H), 7.56 (s, 1H), 8.46 (s, 1H); ¹³C NMR (150 MHz, CDCl₃) δ 14.3, 51.3, 55.3, 62.7, 109.1, 113.7, 114.2, 118.8 (q, ¹*J*_{C-F} = 319 Hz, C_F3), 128.0, 130.0, 133.8, 136.3, 148.3, 154.5, 159.7, 163.4; HRMS (ESI+) calcd for C₁₈H₁₇F₃N₃O₆S [M + H]⁺ 460.0785, found 460.0762 (error 5.0 ppm).

Ethyl 1-(4-methoxybenzyl)-6-phenyl-1H-pyrazolo[3,4-b]pyridine-4-carboxylate (111):

A mixture of **110** (0.50 g, 1.08 mmol, 1.0 equiv), Pd(PPh₃)₄ (62.5 mg, 0.054 mmol, 0.05 equiv), Cs₂CO₃ (0.704 g, 2.16 mmol, 2.0 equiv), PhB(OH)₂ (0.198 g, 1.62 mmol, 1.5 equiv) and dioxane (20 mL) was stirred at 100 °C for 5 h. The reaction mixture was cooled to rt, filtered through a plug of Celite and concentrated. Purification by flash chromatography (7:3 hexanes/EtOAc) afforded the title compound (0.39 g, 96%) as a white solid: *R*_f 0.49 (7:3 hexanes/EtOAc); ¹H NMR (600 MHz, CDCl₃) δ 1.50 (t, *J* = 7.2 Hz, 3H), 3.76 (s, 3H), 4.53 (q, *J* = 7.2 Hz, 2H), 5.74 (s, 2H), 6.84 (d, *J* = 9.0 Hz, 2H), 7.40 (d, *J* = 9.0 Hz, 2H), 7.49 (t, *J* = 7.2 Hz, 1H), 7.55 (t, *J* = 7.2 Hz, 2H), 8.22 (d, *J* = 7.2 Hz, 2H), 8.25 (s, 1H), 8.39 (s, 1H); ¹³C NMR (150 MHz, CDCl₃) δ 14.5, 50.6, 55.3, 62.0, 112.1, 114.1, 115.4, 127.7, 129.0, 129.3, 129.8, 129.9, 132.0, 133.2, 138.6, 151.6, 156.9, 159.4, 165.4; HRMS (ESI+) calcd for C₂₃H₂₂N₃O₃ [M + H]⁺ 388.1656, found 388.1666 (error 2.6 ppm).

1-(4-Methoxybenzyl)-6-phenyl-1H-pyrazolo[3,4-b]pyridine-4-carboxylic acid (31):

To a solution of **111** (25 mg, 0.065 mmol) in THF (1 mL) was added 1 N aqueous NaOH (2 mL). The resulting solution was stirred at rt for 3 h. The solvent was partially evaporated, the reaction mixture diluted with H₂O (10 mL) and the pH adjusted to 4–5 with 1 N aqueous HCl. The resulting suspension was extracted with EtOAc (3 × 15 mL), the combined organic layers were washed with saturated aqueous NaCl, dried (MgSO₄), and concentrated to afford the title compound (23 mg, 98%) as a white solid: ¹H NMR (600 MHz, DMSO-*d*₆) δ 3.69 (s, 3H), 5.71 (s, 2H), 6.88 (d, *J* = 9.0 Hz, 2H), 7.31 (d, *J* = 9.0 Hz, 2H), 7.53 (t, *J* = 7.2 Hz, 1H), 7.58 (t, *J* = 7.2 Hz, 2H), 8.21 (s, 1H), 8.27 (d, *J* = 7.2 Hz, 2H), 8.37 (s, 1H); ¹³C NMR (150 MHz, DMSO-*d*₆) δ 49.8, 55.0, 111.9, 113.9, 114.7, 127.3, 129.06, 129.18, 129.25, 130.0, 132.5, 133.3, 137.8, 150.9, 155.9, 158.7, 166.0; HRMS (ESI+) calcd for C₂₁H₁₆N₃O₃ [M – H][–] 358.1197, found 358.1200 (error 0.8 ppm).

1-(4-Hydroxybenzyl)-6-phenyl-1H-pyrazolo[3,4-b]pyridine-4-carboxylic acid (32):

To a solution of **111** (20 mg, 0.052 mmol, 1.0 equiv) in CH₂Cl₂ (2 mL) was added dropwise neat boron trifluoride–dimethylsulfide complex (55 μL, 0.052 mmol, 1.0 equiv) at 0 °C then the reaction was stirred at rt for 18 h. The reaction mixture was slowly poured over ice cold 0.5 M aqueous HCl (10 mL) and extracted with EtOAc (3 × 20 mL). The combined organic layers were washed with saturated aqueous NaHCO₃ (10 mL), H₂O (10 mL), saturated aqueous NaCl (10 mL), dried (MgSO₄) and concentrated. The residue was dissolved in THF (1.0 mL) then 1 N aqueous NaOH (1.0 mL) was added and the resulting solution was stirred at rt for 2 h. The mixture was concentrated and the residue was purified by preparative reverse-phase HPLC (solvent A: 10 mM NH₄·HCO₃, pH 7.5, solvent B: MeCN) using a linear gradient of 20%B to 100%B over 20 min (see General Methods and Materials for further details) to afford the title compound (3.0 mg, 17%) as a white solid: *R*_T 9.6 min; ¹H NMR (600 MHz, CD₃OD) δ 5.68 (s, 2H), 6.71 (d, *J* = 8.4 Hz, 2H), 7.25 (d, *J* = 8.4 Hz, 2H), 7.49 (t, *J* = 7.2 Hz, 1H), 7.54 (t, *J* = 7.2 Hz, 2H), 8.23 (ovlp d, *J* = 7.2 Hz, 2H), 8.24 (ovlp s, 1H), 8.40 (s, 1H); ¹³C NMR (150 MHz, CD₃OD) δ 51.4, 113.9, 116.2, 116.3, 128.6, 129.4, 130.0, 130.5, 130.8, 134.3, 134.5, 140.1, 152.7, 158.2, 158.6, 165.2; HRMS (ESI–) calcd for C₂₀H₁₄N₃O₃ [M – H][–] 344.1041, found 344.1038 (error 0.9 ppm).

Ethyl 6-phenyl-1H-pyrazolo[3,4-b]pyridine-4-carboxylate (112): A mixture of **111** (340 mg, 0.88 mmol) and TFA (4 mL) was heated at 70 °C for 24 h. Evaporation under vacuum followed by purification of the residue by flash chromatography (7:3 hexanes/EtOAc) afforded the title compound (199 mg, 85%) as a white solid: *R*_f 0.51 (3:2 hexanes/EtOAc); ¹H NMR (600 MHz, CDCl₃) δ 1.53 (t, *J* = 7.2 Hz, 3H), 4.57 (q, *J* = 7.2 Hz, 2H), 7.51 (t, *J* = 7.2 Hz, 1H), 7.56 (t, *J* = 7.2 Hz, 2H), 8.16 (d, *J* = 7.2 Hz, 2H), 8.28 (s, 1H), 8.52 (s, 1H); ¹³C NMR (150 MHz, CDCl₃) δ 14.5, 62.2, 111.8, 116.2, 127.9, 129.2, 130.1, 132.4,

135.1, 138.6, 153.4, 158.0, 165.3; HRMS (ESI+) calcd for C₁₅H₁₄N₃O₂ [M + H]⁺ 268.1081, found 268.1056 (error 9.3 ppm).

6-Phenyl-1*H*-pyrazolo[3,4-*b*]pyridine-4-carboxylic acid (36): To a solution of **112** (30 mg, 0.11 mmol) in THF (1.0 mL) was added 1 N aqueous NaOH (0.6 mL). The resultant solution was stirred at rt for 5 h. The mixture was concentrated and the residue was purified by preparative reverse-phase HPLC (solvent A: 10 mM NH₄-HCO₃, pH 7.5, solvent B: MeCN) using a linear gradient of 10%B to 40%B over 20 min (see General Methods and Materials for further details) to afford the title compound (23 mg, 86%) as a white solid: R_T 18.9 min; ¹H NMR (600 MHz, CD₃OD) δ 7.45 (t, *J* = 7.2 Hz, 1H), 7.51 (t, *J* = 7.2 Hz, 2H), 8.13 (s, 1 H), 8.15 (d, *J* = 7.2 Hz, 2H), 8.47 (s, 1H); ¹³C NMR (150 MHz, CD₃OD) δ 113.8, 115.8, 128.6, 129.8, 130.5, 135.9, 140.7, 142.2, 150.3, 159.9, 172.5; HRMS (ESI-) calcd for C₁₃H₈N₃O₂ [M - H]⁻, 238.0622; found 238.0617 (error 2.1 ppm).

1-(4-Methoxybenzyl)-6-(phenylamino)-1*H*-pyrazolo[3,4-*b*]pyridine-4-carboxylic acid (100): A mixture of **110** (100 mg, 0.22 mmol, 1.0 equiv), Pd(OAc)₂ (5 mg, 0.022 mmol, 0.1 equiv), BINAP (20.4 mg, 0.033 mmol, 0.15 equiv), Cs₂CO₃ (107 mg, 0.33 mmol, 1.5 equiv), aniline (30 μL, 0.33 mmol, 1.5 equiv) and dioxane (1.5 mL) in a pressure vessel was stirred at 100 °C for 22 h. The reaction mixture was cooled to rt, diluted with EtOAc (10 mL), filtered through a plug of Celite and concentrated. Purification by flash chromatography (4:1 hexanes/EtOAc) afforded ethyl 1-(4-methoxybenzyl)-6-(phenylamino)-1*H*-pyrazolo[3,4-*b*]pyridine-4-carboxylate (83 mg, 90%) as a light yellow solid: R_f 0.53 (3:2 hexanes/EtOAc); ¹H NMR (600 MHz, CDCl₃) δ 1.45 (t, *J* = 7.2 Hz, 3H), 3.76 (s, 3H), 4.46 (q, *J* = 7.2 Hz, 2H), 5.55 (s, 2H), 6.84 (d, *J* = 8.4 Hz, 2H), 6.87 (br s, 1H, NH), 7.11 (t, *J* = 7.8 Hz, 1H), 7.22 (s, 1H), 7.33 (d, *J* = 8.4 Hz, 2H), 7.38 (t, *J* = 7.8 Hz, 2H), 7.63 (d, *J* = 7.8 Hz, 2H), 8.18 (s, 1H); ¹³C NMR (150 MHz, CDCl₃) δ 14.5, 50.7, 55.5, 62.1, 107.5, 108.6, 114.2, 120.1, 123.4, 129.4, 129.6, 129.7, 133.2, 133.6, 140.1, 150.9, 155.1, 159.4, 165.4.

To a solution of ethyl 1-(4-methoxybenzyl)-6-(phenylamino)-1*H*-pyrazolo[3,4-*b*]pyridine-4-carboxylate prepared above (30 mg, 0.074 mmol) in THF (1.0 mL) was added 1 N aqueous NaOH (2 mL). The resulting solution was stirred at rt for 3 h. The mixture was concentrated and H₂O (10 mL) was added to the residue. The pH was adjusted to 4–5 with 1 N aqueous HCl and the solution extracted with EtOAc (3 × 15 mL). The combined organic layers were dried (MgSO₄) and concentrated. Purification by flash chromatography (3:7 EtOAc/MeOH) afforded the title compound (19 mg, 69%) as a yellow solid: ¹H NMR (600 MHz, CDCl₃) δ 3.72 (s, 3H), 5.47 (s, 2H), 6.83 (d, *J* = 9.0 Hz, 2H), 6.97 (t, *J* = 7.8 Hz, 1H), 7.16 (s, 1H), 7.26 (d, *J* = 9.0 Hz, 2H), 7.29 (t, *J* = 7.8 Hz, 2H), 7.79 (d, *J* = 7.8 Hz, 2H), 8.23 (s, 1H); ¹³C NMR (150 MHz, CDCl₃) δ 51.1, 55.7, 108.9, 110.2, 114.9, 120.1, 122.8, 129.7, 130.1, 131.0, 135.0, 141.3, 142.5, 151.9, 157.5, 160.7, 173.2; HRMS (ESI-) calcd for C₂₁H₁₇N₄O₃ [M - H]⁻ 373.1306, found 373.1282 (error 6.4 ppm).

Compounds from Scheme 3—See Supporting Information for the experimental details and data for **37–41**, **43–62**, and **66–92**, which were prepared analogously to **15** and **42**, whose experimentals are included below as representative examples.

General Procedure for Suzuki Coupling of 109: To a solution of **109** (100 mg, 0.335 mmol, 1.0 equiv) and triethylamine (141 μL, 1.00 mmol, 3.0 equiv) in dioxane (2.5 mL) in an 8 mL heavy-walled screw-cap round-bottom vial was added PyBroP (187 mg, 0.402 mmol, 1.2 equiv). The reaction mixture was shaken on a Glas-Col heater/shaker (Glas-Col LLC, Terre Haute, IN) at rt for 2 h. The desired boronic acid (0.67 mmol, 2.0 equiv), PdCl₂dppf (12 mg, 0.05 equiv) and Na₂CO₃ (0.7 mL of a 0.254 g/mL aqueous solution, 5.0 equiv) were added, the vial was sealed, and heated at 100 °C for 4 h with shaking. The

reaction mixture was cooled to rt and the solvent removed on a Genevac instrument at 45 °C. The residue was resuspended in H₂O (2 mL) and extracted with CH₂Cl₂ (3 mL) using a 6 mL Biotage Isolute phase separator cartridge (Biotage, Charlottesville, Virginia). The organic layer was concentrated and the residue purified by flash chromatography (hexanes/EtOAc gradient) on a Combiflash Companion system, using a 4 g pre-packed silica column, to afford the desired product.

General Procedure for Ester Hydrolysis: To a solution of the ester (typically 50 mg, 1 equiv) in THF (1 mL) in an 8 mL vial was added 1 N aqueous NaOH (5.0 mL, 5 equiv). The resulting cloudy solution was stirred at rt for 4 h. The solvent was removed under vacuum at 45 °C on a Genevac instrument. The residue was resuspended in H₂O (2 mL) and neutralized with 12 N HCl (0.29 mL, 3.5 equiv). Methanol or DMSO were added when necessary to fully dissolve the products, which were purified by preparative reverse-phase HPLC using the indicated methods. Lyophilisation of the fractions containing the product afforded the title compounds.

Ethyl 6-phenyl-1-(pyridin-4-ylmethyl)-1H-pyrazolo[3,4-b]pyridine-4-carboxylate (18):

The title compound was prepared using the general procedure for Suzuki coupling of **109** (0.40 g, 1.34 mmol, 1.0 equiv) using phenylboronic acid (327 mg, 2.68 mmol, 2.0 equiv). Purification by flash chromatography afforded the title compound (326 mg, 74%) as a white solid: *R_f* 0.39 (EtOAc); ¹H NMR (600 MHz, CDCl₃) δ 1.52 (t, *J* = 7.2 Hz, 3H), 4.55 (q, *J* = 7.2 Hz, 2H), 5.82 (s, 2H), 7.22 (d, *J* = 6.0 Hz, 2H), 7.49 (t, *J* = 7.2 Hz, 1H), 7.53 (t, *J* = 7.2 Hz, 2H), 8.17 (d, *J* = 7.2 Hz, 2H), 8.29 (s, 1H), 8.46 (s, 1H), 8.55 (d, *J* = 6.0 Hz, 2H); ¹³C NMR (150 MHz, CDCl₃) δ 14.5, 49.8, 62.2, 112.1, 115.8, 122.6, 127.6, 129.0, 130.1, 132.4, 134.0, 138.3, 145.8, 150.3, 151.9, 157.4, 165.2; HRMS (ESI+) calcd for C₂₁H₁₉N₄O₂ [M + H]⁺ 359.1503; found 359.1527 (error 6.7 ppm).

6-Phenyl-1-(pyridin-4-ylmethyl)-1H-pyrazolo[3,4-b]pyridine-4-carboxylic acid (15):

Compound **18** (120 mg, 0.324 mmol, 1.0 equiv) was converted to the title compound using the general procedure for ester hydrolysis. Purification by preparative reverse-phase HPLC using method 2 followed by lyophilisation of the pooled product fractions afforded the title compound (87 mg, 81%) as a white solid: *R_T* 11.0 min; ¹H NMR (600 MHz, CD₃OD) δ 5.86 (s, 2H), 7.30 (d, *J* = 6.0 Hz, 2H), 7.45 (t, *J* = 7.2 Hz, 1H), 7.50 (t, *J* = 7.2 Hz, 2H), 8.18 (d, *J* = 7.2 Hz, 2H), 8.19 (s, 1H), 8.46 (d, *J* = 6.0 Hz, 2H), 8.53 (s, 1H); ¹³C NMR (150 MHz, CD₃OD) δ 50.3, 114.7, 116.1, 124.1, 128.6, 129.8, 130.6, 135.9, 140.4, 143.1, 149.3, 150.3, 153.2, 158.9, 172.4; HRMS (ESI-) calcd for C₁₉H₁₃N₄O₂ [M - H]⁻ 329.1044, found 329.1040 (error 1.2 ppm).

6-(4-Hydroxyphenyl)-1-(pyridin-4-ylmethyl)-1H-pyrazolo[3,4-b]pyridine-4-carboxylic acid (42): Ethyl 6-(4-hydroxyphenyl)-1-(pyridin-4-ylmethyl)-1H-pyrazolo[3,4-b]pyridine-4-carboxylate (**42-Ethyl ester**) was prepared using the general procedure for Suzuki coupling of **109** with 4-hydroxyphenylboronic acid (92 mg, 0.67 mmol, 2 equiv). Purification by flash chromatography afforded **42-Ethyl ester** (78 mg, 62%) as a white solid: *R_f* 0.22 (EtOAc); ¹H NMR (600 MHz, DMSO-*d*₆) δ 1.44 (t, *J* = 7.2 Hz, 3H), 4.49 (q, *J* = 7.2 Hz, 2H), 5.83 (s, 2H), 6.92 (d, *J* = 8.4 Hz, 2H), 7.19 (d, *J* = 5.4 Hz, 2H), 8.10 (d, *J* = 8.4 Hz, 2H), 8.16 (s, 1H), 8.41 (s, 1H), 8.50 (d, *J* = 5.4 Hz, 2H), 9.98 (s, 1H, OH); ¹³C NMR (150 MHz, DMSO-*d*₆) δ 14.1, 48.9, 61.8, 110.6, 114.1, 115.9, 122.2, 128.3, 129.0, 131.9, 133.2, 146.1, 149.9, 151.4, 156.4, 159.6, 164.6.

42-Ethyl ester (50 mg, 0.133 mmol, 1.0 equiv) prepared above was converted to the title compound using the general procedure for ester hydrolysis. Purification by preparative reverse-phase HPLC using method 2 afforded the title compound (43 mg, 93%) as a white

solid: R_T 8.0 min; 1H NMR (600 MHz, CD_3OD) δ 5.83 (s, 2H), 6.89 (d, $J = 8.4$ Hz, 2H), 7.29 (d, $J = 5.4$ Hz, 2H), 8.05 (d, $J = 8.4$ Hz, 2H), 8.11 (s, 1H), 8.46 (d, $J = 5.4$ Hz, 2H), 8.48 (s, 1H); ^{13}C NMR (150 MHz, CD_3OD) δ 50.2, 113.9, 115.5, 116.7, 124.1, 130.1, 131.5, 142.8, 149.4, 150.3, 153.2, 159.1, 159.4, 160.8, 172.6; HRMS (ESI $^-$) calcd for $C_{19}H_{13}N_4O_3$ $[M - H]^-$ 345.0993, found 345.0999 (error 1.7 ppm).

General procedure for Amination of 109: To a solution of **109** (100 mg, 0.335 mmol, 1.0 equiv) and BOP (193 mg, 0.437 mmol, 1.3 equiv) in dioxane (3 mL) in an 8 mL vial was added DBU (76 μ L, 0.504 mmol, 1.5 equiv) and the resulting mixture was stirred for 15 min at rt. The desired amine (1.01 mmol, 3 equiv) was added, the vial was sealed, and the reaction mixture was heated at 70 $^\circ$ C with stirring for 5 h. The reaction mixture was concentrated, then the residue was resuspended in H_2O (10 mL) and extracted with EtOAc (3 \times 15 mL). The combined organic layers were dried ($MgSO_4$) and concentrated. Purification by flash chromatography (hexane/EtOAc gradient) on a Combiflash Companion system, using a 4 g pre-packed silica column, afforded the desired product.

6-(Benzylamino)-1-(pyridin-4-ylmethyl)-1H-pyrazolo[3,4-b]pyridine-4-carboxylic acid

(95): Ethyl 6-(benzylamino)-1-(pyridin-4-ylmethyl)-1H-pyrazolo[3,4-b]pyridine-4-carboxylate was prepared using the general procedure for amination of **109** with benzylamine (110 μ L, 1.01 mmol, 3 equiv). Purification by flash chromatography afforded the ethyl ester of the title compound (28 mg, 22%) as a white solid: R_T 0.42 (EtOAc); 1H NMR (600 MHz, $CDCl_3$) δ 1.44 (t, $J = 7.2$ Hz, 3H), 4.43 (q, $J = 7.2$ Hz, 2H), 4.66 (d, $J = 6.0$ Hz, 2H), 5.50 (ovlp t, $J = 6.0$ Hz, 1H, NH), 5.52 (ovlp s, 2H), 7.02 (s, 1H), 7.07 (d, $J = 5.4$ Hz, 2H), 7.26 (t, $J = 7.2$ Hz, 1H), 7.29 (t, $J = 7.2$ Hz, 2H), 7.33 (d, $J = 7.2$ Hz, 2H), 8.15 (s, 1H), 8.46 (d, $J = 5.4$ Hz, 2H); ^{13}C NMR (150 MHz, $CDCl_3$) δ 14.4, 45.9, 49.4, 61.9, 105.1, 108.3, 122.7, 127.5, 127.7, 128.8, 132.9, 134.2, 139.0, 146.3, 150.0, 151.7, 158.0, 165.4.

Ethyl 6-(benzylamino)-1-(pyridin-4-ylmethyl)-1H-pyrazolo[3,4-b]pyridine-4-carboxylate prepared above (20 mg, 0.052 mmol, 1.0 equiv) was converted to the title compound using the general procedure for ester hydrolysis. Purification by preparative reverse-phase HPLC using method 4 afforded the title compound as a white solid (17 mg, 91%): R_T 10.0 min; 1H NMR (600 MHz, CD_3OD) δ 4.60 (s, 2H), 5.51 (s, 2H), 6.92 (s, 1H), 7.10 (d, $J = 6.0$ Hz, 2H), 7.17 (t, $J = 7.2$ Hz, 1H), 7.21 (t, $J = 7.2$ Hz, 2H), 7.31 (d, $J = 7.2$ Hz, 2H), 8.13 (s, 1H), 8.34 (d, $J = 6.0$ Hz, 2H); ^{13}C NMR (150 MHz, $DMSO-d_6$) δ 44.2, 48.5, 104.9, 122.3, 122.5, 127.4, 127.7, 128.0, 128.3, 139.8, 146.4, 149.6, 149.8, 151.2, 158.3, 166.3; HRMS (ESI $^-$) calcd for $C_{20}H_{16}N_5O_2$ $[M - H]^-$ 358.1309, found 358.1316 (error 2.0 ppm).

6-Morpholino-1-(pyridin-4-ylmethyl)-1H-pyrazolo[3,4-b]pyridine-4-carboxylic acid

(96): Ethyl 6-morpholino-1-(pyridin-4-ylmethyl)-1H-pyrazolo[3,4-b]pyridine-4-carboxylate was prepared using the general procedure for amination of **109** with morpholine (88 μ L, 1.01 mmol, 3 equiv). Purification by flash chromatography afforded the ethyl ester of the title compound (98 mg, 79%) as a pale yellow solid: R_T 0.37 (EtOAc); 1H NMR (600 MHz, $CDCl_3$) δ 1.48 (t, $J = 7.2$ Hz, 3H), 3.68 (t, $J = 4.8$ Hz, 4H), 3.83 (t, $J = 4.8$ Hz, 4H), 4.49 (q, $J = 7.2$ Hz, 2H), 5.56 (s, 2H), 7.12 (d, $J = 6.0$ Hz, 2H), 7.27 (s, 1H), 8.18 (s, 1H), 8.52 (d, $J = 6.0$ Hz, 2H); ^{13}C NMR (150 MHz, $CDCl_3$) δ 14.5, 45.8, 49.4, 62.1, 66.8, 105.5, 106.3, 122.6, 133.3, 134.2, 146.4, 150.1, 151.5, 158.9, 165.6.

Ethyl 6-morpholino-1-(pyridin-4-ylmethyl)-1H-pyrazolo[3,4-b]pyridine-4-carboxylate prepared above (98 mg, 0.267 mmol, 1.0 equiv) was converted to the title compound using the general procedure for ester hydrolysis. Purification by preparative reverse-phase HPLC using method 4 afforded the title compound (45 mg, 97%) as a pale yellow solid: R_T 6.5 min; 1H NMR (600 MHz, $DMSO-d_6$) δ 3.62 (t, $J = 4.8$ Hz, 4H), 3.70 (t, $J = 4.8$ Hz, 4H), 5.56 (s, 2H), 7.14 (d, $J = 6.0$ Hz, 2H), 7.26 (s, 1H), 8.10 (s, 1H), 8.48 (d, $J = 6.0$ Hz,

2H); ^{13}C NMR (150 MHz, CD_3OD) δ 45.2, 48.6, 65.9, 105.1, 105.7, 122.4, 133.2, 133.9, 146.4, 149.8, 150.9, 158.6, 166.3; HRMS (ESI $^-$) calcd for $\text{C}_{17}\text{H}_{16}\text{N}_5\text{O}_3$ $[\text{M} - \text{H}]^-$ 338.1259, found 338.1262 (error 0.9 ppm).

6-(3-Hydroxypropylamino)-1-(pyridin-4-ylmethyl)-1H-pyrazolo[3,4-*b*]pyridine-4-carboxylic acid (97): Ethyl 6-(3-hydroxypropylamino)-1-(pyridin-4-ylmethyl)-1H-pyrazolo[3,4-*b*]pyridine-4-carboxylate was prepared using the general procedure for amination of **109** with 3-hydroxypropylamine (77 μL , 1.01 mmol, 3 equiv). The crude product obtained after extraction was converted to the title compound using the general procedure for ester hydrolysis. Purification by preparative reverse-phase HPLC using method 4 afforded the title compound (22 mg, 18% over 2 steps) as a white solid: R_T 8.6 min; ^1H NMR (600 MHz, $\text{DMSO-}d_6$) δ 1.70 (pent, $J = 6.6$ Hz, 2H), 3.37 (t, $J = 6.6$ Hz, 2H), 3.48 (t, $J = 6.6$ Hz, 2H), 5.50 (s, 2H), 7.01 (s, 1H), 7.15 (d, $J = 4.8$ Hz, 2H), 7.98 (s, 1H), 8.47 (d, $J = 4.8$ Hz, 2H); ^{13}C NMR (150 MHz, $\text{DMSO-}d_6$) δ 31.9, 38.0, 48.7, 58.7, 99.5, 104.6, 122.6, 132.5, 133.3, 146.8, 149.8, 151.8, 158.8, 166.4; HRMS (ESI $^-$) calcd for $\text{C}_{16}\text{H}_{16}\text{N}_5\text{O}_3$ $[\text{M} - \text{H}]^-$ 326.1259, found 326.1260 (error 0.3 ppm).

6-Oxo-1-(pyridin-4-ylmethyl)-6,7-dihydro-1H-pyrazolo[3,4-*b*]pyridine-4-carboxylic acid (98): Compound **109** (40 mg, 0.134 mmol, 1.00 equiv) was converted to the title compound using the general procedure for ester hydrolysis. Purification by preparative HPLC using method 5 afforded the title compound (26 mg, 72%) as a white solid: $R_T = 8.0$ min; ^1H NMR (600 MHz, CD_3OD) δ 5.59 (s, 2H), 6.86 (s, 1H), 7.17 (d, $J = 6.0$ Hz, 2H), 8.21 (s, 1H), 8.44 (d, $J = 6.0$ Hz, 2H); ^{13}C NMR (150 MHz, CD_3OD) δ 50.0, 108.4, 111.5, 123.8, 136.4, 144.9, 149.5, 150.2, 150.9, 169.5, 172.8; HRMS (ESI $^-$) calcd for $\text{C}_{13}\text{H}_9\text{N}_4\text{O}_3$ $[\text{M} - \text{H}]^-$ 269.0680, found 269.0682 (error 0.7 ppm).

Compounds from Scheme 4—See Supporting Information for the experimental details and data for **60** and **64–65**, which were prepared analogously to **43**, whose experimentals are included below as a representative example.

General Procedure for Alkylation of 42-Ethyl ester and Hydrolysis: To a solution of **42-Ethyl ester** (112.3 mg, 0.30 mmol, 1.0 equiv) and Na_2CO_3 (63.6 mg, 0.6 mmol, 2.0 equiv) in 1:1 dioxane– H_2O (6 mL) was added the respective alkylbromide (1.2 mmol, 4.0 equiv). The mixture was heated at 80 $^\circ\text{C}$ for 12 h, then cooled to rt and the crude mixture was extracted with EtOAc (3 \times 15 mL). The combined organic layers were washed with saturated aqueous NaCl (20 mL), dried (MgSO_4), and concentrated. The crude residue was purified by flash chromatography (4:1 EtOAc–hexane) to afford the ethyl esters of the title compounds. Hydrolysis of the ethyl esters was accomplished by dissolving the intermediate ethyl esters (0.30 mmol, 1.0 equiv) in THF (3 mL) followed by the addition of 1 N aqueous NaOH (3 mL, 3 mmol, 10 equiv). The resulting solution was stirred at 60 $^\circ\text{C}$ for 12 h, then cooled to rt. The pH was adjusted to ~ 6 by the addition of 1 N aqueous HCl and the crude mixture was extracted with 10:1 EtOAc–MeOH (5 \times 15 mL). The combined organic extracts were washed with saturated aqueous NaCl (20 mL), dried (MgSO_4), and concentrated. The products were dissolved in EtOAc with a small amount of MeOH to aid in dissolution then triturated with hexane, whereupon the products precipitated as analytically pure white solids in yields ranging from 40–70%.

6-[4-(Octyloxy)phenyl]-1-(pyridin-4-ylmethyl)-1H-pyrazolo[3,4-*b*]pyridine-4-carboxylic acid (63): The title compound was prepared using the general procedure for alkylation of **42-Ethyl ester** and hydrolysis employing octylbromide (210 μL , 1.2 mmol) to afford the title compound (38 mg, 28% over two steps) as a white solid: R_T 0.22 (1:4 MeOH/EtOAc); ^1H NMR (600 MHz, $\text{DMSO-}d_6$) δ 0.86 (t, $J = 7.2$ Hz, 3H), 1.27–1.32 (m, 8H),

1.41–1.42 (m, 2H), 1.72–1.75 (m, 2H), 4.04 (t, $J = 7.2$ Hz, 2H), 5.84 (s, 2H), 7.07 (d, $J = 8.2$ Hz, 2H), 7.20 (d, $J = 3.2$ Hz, 2H), 8.17–8.19 (m, 3H), 8.41 (s, 1H), 8.50 (d, $J = 3.2$ Hz, 2H); ^{13}C NMR (150 MHz, DMSO- d_6) δ 14.0, 22.1, 25.5, 28.62, 28.65, 28.7, 31.2, 48.9, 67.6, 111.6, 114.3, 114.8, 122.3, 128.8, 130.0, 133.5, 141.5, 146.2, 149.9, 151.4, 156.0, 160.3, 170.4; HRMS (ESI $^-$) calcd for $\text{C}_{27}\text{H}_{29}\text{N}_4\text{O}_3$ $[\text{M} - \text{H}]^-$ 457.2245, found 457.2220 (error 5.5 ppm).

6-Ethynyl-1-(pyridin-4-ylmethyl)-1H-pyrazolo[3,4-*b*]pyridine-4-carboxylic acid (93): A 1.0 M solution of TBAF in THF (0.25 mL, 1.0 equiv) was added to a solution of **114**⁴⁵ (105 mg, 0.25 mmol, 1.0 equiv) in THF (10 mL) at 0 °C and stirred for 3 h. The reaction mixture was diluted with H₂O (10 mL) and extracted with CH₂Cl₂ (3 × 15 mL). The combined organic layers were dried (MgSO₄), and concentrated. Purification by flash chromatography (hexane–EtOAc gradient) afforded **116** (27 mg, 35%) as a white solid: R_f 0.54 (EtOAc); ^1H NMR (600 MHz, CDCl₃) δ 1.48 (t, $J = 7.2$ Hz, 3H), 3.32 (s, 1H), 4.52 (q, $J = 7.2$ Hz, 2H), 5.75 (s, 2H), 7.13 (d, $J = 4.8$ Hz, 2H), 7.94 (s, 1H), 8.48 (s, 1H), 8.53 (d, $J = 4.8$ Hz, 2H); ^{13}C NMR (150 MHz, CDCl₃) δ 14.4, 49.8, 62.4, 72.3, 82.7, 113.0, 122.0, 122.6, 132.1, 134.1, 141.5, 145.4, 150.3, 151.3, 164.4.

Compound **116** prepared above (20 mg, 0.065 mmol, 1.0 equiv) was converted to the title compound using the general procedure for ester hydrolysis. Purification by preparative reverse-phase HPLC using method 4 afforded the title compound (7.4 mg, 41%) as an off-white solid: R_T 8.3 min; ^1H NMR (400 MHz, DMSO- d_6) δ 4.64 (s, 1H), 5.78 (s, 2H), 7.12 (d, $J = 6.0$ Hz, 2H), 7.74 (s, 1H), 8.50 (d, $J = 6.0$ Hz, 2H), 8.51 (s, 1H); ^{13}C NMR (100 MHz, DMSO- d_6) δ 49.0, 82.4, 82.8, 99.5, 112.9, 121.0, 122.0, 133.7, 140.7, 145.9, 149.9, 150.8, 165.3; HRMS (ESI $^-$) calcd for $\text{C}_{15}\text{H}_9\text{N}_4\text{O}_2$ $[\text{M} - \text{H}]^-$ 277.0731, found 277.0736 (error 1.8 ppm).

6-(Phenylethynyl)-1-(pyridin-4-ylmethyl)-1H-pyrazolo[3,4-*b*]pyridine-4-carboxylic acid (94): Compound **115**⁴⁵ (60 mg, 0.157 mmol, 1.0 equiv) was converted to the title compound using the general procedure for ester hydrolysis. Purification by preparative reverse-phase HPLC using method 2 afforded the title compound (36 mg, 65%) as a white solid: R_T 11.8 min; ^1H NMR (600 MHz, DMSO- d_6) δ 5.77 (s, 2H), 7.10 (d, $J = 5.4$ Hz, 2H), 7.45–7.50 (m, 3H), 7.68 (dd, $J = 7.8, 2.4$ Hz, 2H), 7.77 (s, 1H), 8.49 (d, $J = 5.4$ Hz, 2H), 8.54 (s, 1H); ^{13}C NMR (150 MHz, DMSO- d_6) δ 48.9, 89.5, 89.6, 113.7, 121.1, 121.2, 121.9, 128.9, 129.7, 131.9, 134.7, 141.1, 146.4, 149.8, 151.1, 165.8 (missing one aryl carbon); HRMS (ESI $^-$) calcd for $\text{C}_{21}\text{H}_{13}\text{N}_4\text{O}_2$ $[\text{M} - \text{H}]^-$ 353.1044, found 353.1035 (error 2.5 ppm).

Compounds from Scheme 5—See Supporting Information for the experimental details and data for **23–25**, **27–28**, which were prepared analogously to **22**, whose experimental is included below as a representative example.

4-Hydroxymethyl-6-phenyl-1-(pyridin-4-ylmethyl)-1H-pyrazolo[3,4-*b*]pyridine (19): A solution of **18** (358 mg, 1.0 mmol, 1.0 equiv) in THF (2 mL) was slowly added to a suspension of LiAlH₄ (57 mg, 1.5 mmol, 1.5 equiv) in THF (8.0 mL) at 0 °C. The reaction mixture was stirred at 0 °C for 10 min and gradually warmed up to 22 °C over 1 h. After stirring for 2 h at 22 °C, the reaction was quenched with MeOH (5 mL) and diluted with CH₂Cl₂ (15 mL). The organic layer was washed consecutively with saturated aqueous NH₄Cl (10 mL), H₂O (10 mL), saturated aqueous NaCl (10 mL), then dried (Na₂SO₄) and concentrated. Purification by flash chromatography (10:1 to 5:1 CH₂Cl₂–MeOH) afforded the title compound **19** (143 mg, 45%) as a white solid: R_f 0.36 (EtOAc); ^1H NMR (600 MHz, CDCl₃) δ 5.09 (s, 2H), 5.75 (s, 2H), 7.15 (d, $J = 6.0$ Hz, 2H), 7.43 (t, $J = 7.2$ Hz, 1H), 7.47 (t, $J = 7.2$ Hz, 2H), 7.65 (s, 1H), 8.08 (d, $J = 7.2$ Hz, 2H), 8.16 (s, 1H), 8.42 (d, $J = 6.0$

Hz, 2H); ^{13}C NMR (150 MHz, CDCl_3) δ 49.5, 62.7, 111.7, 112.6, 122.8, 127.6, 128.9, 129.7, 132.3, 139.2, 146.2, 146.6, 149.8, 151.3, 157.4; HRMS (ESI+) calcd for $\text{C}_{19}\text{H}_{17}\text{N}_4\text{O}$ $[\text{M}]^+$ 317.1397, found 317.1395 (error 0.6 ppm).

6-Phenyl-1-(pyridin-4-ylmethyl)-1H-pyrazolo[3,4-b]pyridin-4-amine (21): Compound **15** (50 mg, 0.168 mmol, 1.0 equiv) was dissolved in 3:1 CH_2Cl_2 -THF (4 mL), and oxalyl chloride (17.6 μL , 0.205 mmol, 1.2 equiv) was slowly added at rt. The reaction mixture was stirred for 4 h then concentrated in vacuo. The residue was dissolved in acetone (5 mL) and added to a solution of NaN_3 (47 mg, 0.73 mmol, 4.3 equiv) in H_2O (5 mL). The solution was immediately extracted with EtOAc (2×20 mL). The combined organic layers were dried (MgSO_4) and the solvent removed under vacuum. The residue was dissolved in benzene (5 mL), then TFA (19 μL , 0.25 mmol, 1.5 equiv) was added, and the solution was refluxed for 16 h. The solution was concentrated and the residue redissolved in MeOH (5 mL). Solid K_2CO_3 (51 mg, 0.37 mmol, 2.2 equiv) was added and the reaction mixture was stirred vigorously for 8 h at rt. The mixture was concentrated and the residue partitioned between H_2O (10 mL) and EtOAc (3×15 mL). The combined organic layers were dried (MgSO_4) and the solvent removed under vacuum. Purification by flash chromatography (hexanes/EtOAc gradient) afforded the title compound (16 mg, 31%) as a white solid: R_f 0.36 (EtOAc); ^1H NMR (600 MHz, CDCl_3) δ 4.80 (br s, 2H, NH_2), 5.70 (s, 2H), 6.78 (s, 1H), 7.21 (d, $J = 4.8$ Hz, 2H), 7.41 (t, $J = 7.2$ Hz, 1H), 7.46 (t, $J = 7.2$ Hz, 2H), 7.97 (s, 1H), 8.02 (d, $J = 7.2$ Hz, 2H), 8.54 (br s, 2H); ^{13}C NMR (150 MHz, CDCl_3) δ 49.6, 98.5, 104.7, 122.8, 127.5, 128.7, 129.3, 130.2, 139.9, 146.5, 148.2, 150.1, 152.9, 158.6; HRMS (ESI-) calcd for $\text{C}_{18}\text{H}_{14}\text{N}_5\text{O}$ $[\text{M} - \text{H}]^-$ 300.1255, found 300.1255 (error 0 ppm).

General procedure for the synthesis of 6-phenyl-1-(pyridin-4-ylmethyl)-1H-pyrazolo[3,4-b]pyridine-4-carboxamide analogues: To a solution of **15** (15 mg, 0.045 mmol, 1.0 equiv) and DMF (3.5 μL , 0.045 mmol, 1.0 equiv) in dry CH_2Cl_2 (2 mL) at 0 °C was added oxalyl chloride (7.7 μL , 0.090 mmol, 2.0 equiv). The reaction was stirred for 1 hour, then concentrated in vacuo. A solution of the desired amine (2–10 equiv) and DMAP (1.8 mg, 0.015 mmol, 0.3 equiv) in CH_2Cl_2 (2.0 mL) were added and the reaction was stirred 1 h at rt. The mixture was concentrated and the residue resuspended in H_2O (2 mL). Methanol or DMSO were added if necessary to fully dissolve the products. Purification by preparative HPLC using method 2, followed by lyophilization of the pooled product fractions afforded the title compounds.

6-Phenyl-1-(pyridin-4-ylmethyl)-1H-pyrazolo[3,4-b]pyridine-4-carboxamide (22): The title compound was prepared using the general procedure for the synthesis of 4-carboxamide analogues from **15**, using a 14.8 M ammonium hydroxide solution (34 μL , 0.50 mmol, 10 equiv). Purification by preparative reverse-phase HPLC using method 2 afforded the title compound (4.9 mg, 30%) as a white solid: R_T 12.2 min; ^1H NMR (600 MHz, CD_3OD) δ 5.88 (s, 2H), 7.32 (d, $J = 5.4$ Hz, 2H), 7.48 (t, $J = 7.2$ Hz, 1H), 7.52 (t, $J = 7.2$ Hz, 2H), 8.17 (s, 1H), 8.23 (d, $J = 7.2$ Hz, 2H), 8.45 (s, 1H), 8.47 (d, $J = 5.4$ Hz, 2H); ^{13}C NMR (150 MHz, CD_3OD) δ 50.4, 113.2, 114.3, 124.1, 128.7, 130.0, 131.1, 134.7, 138.3, 139.7, 149.0, 150.4, 153.0, 159.1, 169.9; HRMS (ESI+) calcd for $\text{C}_{19}\text{H}_{16}\text{N}_5\text{O}$ $[\text{M} + \text{H}]^+$ 330.1349, found 330.1353 (error 1.2 ppm).

Compounds from Scheme 6

Methyl 6-bromo-1-(pyridin-4-ylmethyl)-1H-indazole-4-carboxylate (119) and Methyl 6-bromo-2-(pyridin-4-ylmethyl)-2H-indazole-4-carboxylate (121): To a solution of methyl 6-bromo-1H-indazole-4-carboxylate **117** (300 mg, 1.18 mmol, 1.0 equiv) in DMF (10 mL) was added Cs_2CO_3 (2.3 g, 7.1 mmol, 6.0 equiv) and the resulting suspension was stirred at rt for 30 min. 4-(Bromomethyl)pyridine hydrobromide (0.89 g, 3.53 mmol, 3.0 equiv) was

added and stirring continued at rt for 3 h. The reaction mixture was diluted with EtOAc (20 mL), filtered through a bed of Celite, and concentrated. Purification by flash chromatography (hexanes/EtOAc gradient) afforded the two title compounds as white solids:

Data for **119** (128 mg, 31%): R_f 0.37 (EtOAc); ^1H NMR (600 MHz, CDCl_3) δ 4.01 (s, 3H), 5.58 (s, 2H), 6.98 (d, $J = 6.0$ Hz, 2H), 7.65 (s, 1H), 8.01 (s, 1H), 8.52–8.54 (m, 3H); ^{13}C NMR (150 MHz, CDCl_3) δ 51.9, 52.7, 116.3, 120.4, 121.7, 122.0, 124.4, 127.9, 135.3, 140.9, 145.1, 150.5, 165.4; HRMS (ESI+) calcd for $\text{C}_{15}\text{H}_{13}\text{BrN}_3\text{O}_2$ $[\text{M} + \text{H}]^+$ 348.0186, found 348.0176 (error 2.8 ppm).

Data for **121** (76 mg, 19%): R_f 0.19 (EtOAc); ^1H NMR (600 MHz, CDCl_3) δ 3.95 (s, 3H), 5.60 (s, 2H), 7.07 (d, $J = 6.0$ Hz, 2H), 7.97 (s, 1H), 8.09 (s, 1H), 8.47 (s, 1H), 8.57 (d, $J = 6.0$ Hz, 2H); ^{13}C NMR (150 MHz, CDCl_3) δ 52.5, 56.5, 119.2, 119.3, 122.1, 123.9, 125.5, 126.0, 130.0, 144.3, 150.1, 150.6, 165.5; HRMS (ESI+) calcd for $\text{C}_{15}\text{H}_{13}\text{BrN}_3\text{O}_2$ $[\text{M} + \text{H}]^+$ 348.0186, found 348.0175 (error 3.2 ppm).

6-Phenyl-1-(pyridin-4-ylmethyl)-1H-indazole-4-carboxylic acid (16): Methyl 6-phenyl-1-(pyridin-4-ylmethyl)-1H-indazole-4-carboxylate was prepared using the general procedure for Suzuki coupling from **119** (50 mg, 0.144 mmol, 1.0 equiv). Purification by flash chromatography (hexanes/EtOAc gradient) afforded the methyl ester of the title compound (28 mg, 57%) as a white solid: R_f 0.40 (EtOAc); ^1H NMR (600 MHz, CDCl_3) δ 4.06 (s, 3H), 5.69 (s, 2H), 7.03 (d, $J = 6.0$ Hz, 2H), 7.40 (t, $J = 7.2$ Hz, 1H), 7.47 (t, $J = 7.2$ Hz, 2H), 7.61 (d, $J = 7.2$ Hz, 2H), 7.63 (s, 1H), 8.22 (s, 1H), 8.54 (d, $J = 6.0$ Hz, 2H), 8.60 (s, 1H); ^{13}C NMR (150 MHz, CDCl_3) δ 51.9, 52.5, 111.6, 121.7, 122.2, 123.7, 125.0, 127.7, 128.2, 129.2, 135.1, 140.1, 140.3, 141.0, 145.6, 150.5, 166.6.

Methyl 6-phenyl-1-(pyridin-4-ylmethyl)-1H-indazole-4-carboxylate (23 mg, 0.067 mmol, 1.0 equiv) prepared above was converted to the title compound using the general procedure for ester hydrolysis. Purification by preparative reverse-phase HPLC using method 3 afforded the title compound (16 mg, 72%) as a white solid: R_T 9.5 min; ^1H NMR (400 MHz, $\text{DMSO}-d_6$) δ 5.87 (s, 2H), 7.13 (d, $J = 6.0$ Hz, 2H), 7.42 (t, $J = 7.2$ Hz, 1H), 7.51 (t, $J = 7.2$ Hz, 2H), 7.78 (d, $J = 7.2$ Hz, 2H), 8.08 (s, 1H), 8.29 (s, 1H), 8.48–8.50 (m, 3H); ^{13}C NMR (100 MHz, $\text{DMSO}-d_6$) δ 50.6, 111.4, 121.6, 122.0 (2 C), 123.1, 127.3, 127.9, 129.0, 134.4, 138.4, 139.5, 141.1, 146.4, 149.9, 167.2; HRMS (ESI-) calcd for $\text{C}_{20}\text{H}_{14}\text{N}_3\text{O}_2$ $[\text{M} - \text{H}]^-$ 328.1092, found 328.1089 (error 0.9 ppm).

6-Phenyl-2-(pyridin-4-ylmethyl)-2H-indazole-4-carboxylic acid (99): Methyl 6-phenyl-2-(pyridin-4-ylmethyl)-2H-indazole-4-carboxylate was prepared using the general procedure for Suzuki coupling from **121** (50 mg, 0.144 mmol, 1.0 equiv). Purification by flash chromatography (hexanes/EtOAc gradient) afforded the methyl ester of the title compound (38 mg, 77%) as a white solid: R_f 0.22 (EtOAc); ^1H NMR (600 MHz, CDCl_3) δ 3.99 (s, 3H), 5.65 (s, 2H), 7.12 (d, $J = 6.0$ Hz, 2H), 7.39 (t, $J = 7.2$ Hz, 1H), 7.48 (t, $J = 7.2$ Hz, 2H), 7.69 (d, $J = 7.2$ Hz, 2H), 8.13 (s, 1H), 8.24 (s, 1H), 8.51 (s, 1H), 8.59 (d, $J = 6.0$ Hz, 2H); ^{13}C NMR (150 MHz, CDCl_3) δ 52.3, 56.5, 119.8, 120.8, 122.1, 122.9, 125.6, 127.4, 127.5, 127.9, 129.1, 139.1, 140.1, 144.7, 150.3, 150.5, 166.6.

Methyl 6-phenyl-2-(pyridin-4-ylmethyl)-2H-indazole-4-carboxylate (34 mg, 0.099 mmol, 1.0 equiv) prepared above was converted to the title compound using the general procedure for ester hydrolysis. Purification by preparative reverse-phase HPLC using method 3 afforded the title compound (25 mg, 77%) as a white solid: R_T 9.0 min; ^1H NMR (400 MHz, $\text{DMSO}-d_6$) δ 5.82 (s, 2H), 7.24 (d, $J = 6.0$ Hz, 2H), 7.40 (t, $J = 7.2$ Hz, 1H), 7.50 (t, $J = 7.2$ Hz, 2H), 7.77 (d, $J = 7.2$ Hz, 2H), 8.08 (s, 1H), 8.15 (s, 1H), 8.54 (d, $J = 6.0$ Hz, 2H), 8.87

(s, 1H); ^{13}C NMR (100 MHz, DMSO- d_6) δ 55.1, 119.0, 119.6, 122.5, 124.3, 125.3, 126.3, 127.0, 127.7, 129.1, 137.4, 139.8, 145.6, 149.6, 149.9, 167.0; HRMS (ESI $^-$) calcd for $\text{C}_{20}\text{H}_{14}\text{N}_3\text{O}_2$ [M - H] $^-$ 328.1092, found 328.1084 (error 2.4 ppm).

Methyl 6-bromo-1-(pyridin-4-ylmethyl)-1H-indole-4-carboxylate (120): To a solution of methyl 6-bromo-1H-indole-4-carboxylate **118** (50 mg, 0.20 mmol, 1.0 equiv) in DMF (3 mL) was added Cs_2CO_3 (391 mg, 1.2 mmol, 6.0 equiv) and the resulting suspension was stirred at rt for 30 min. 4-(Bromomethyl)pyridine hydrobromide (152 mg, 0.6 mmol, 3.0 equiv) was added and stirring continued at rt for 2 h. The reaction mixture was diluted with EtOAc (10 mL), filtered through a bed of Celite and concentrated. Purification by flash chromatography (hexanes/EtOAc gradient) afforded the title compound (53 mg, 77%) as a white solid: R_f 0.30 (EtOAc); ^1H NMR (600 MHz, CDCl_3) δ 3.98 (s, 3H), 5.32 (s, 2H), 6.89 (d, J = 5.4 Hz, 2H), 7.20 (d, J = 3.0 Hz, 1H), 7.23 (d, J = 3.0 Hz, 1H), 7.50 (s, 1H), 8.01 (s, 1H), 8.53 (d, J = 5.4 Hz, 2H); ^{13}C NMR (150 MHz, CDCl_3) δ 49.3, 52.2, 104.1, 114.8, 116.9, 121.2, 123.3, 125.5, 127.4, 131.1, 137.8, 145.7, 150.6, 166.7; HRMS (ESI $^+$) calcd for $\text{C}_{16}\text{H}_{14}\text{BrN}_2\text{O}_2$ [M + H] $^+$ 347.0213, found 347.0222 (error 2.6 ppm).

6-Phenyl-1-(pyridin-4-ylmethyl)-1H-indole-4-carboxylic acid (17): Methyl 6-phenyl-1-(pyridin-4-ylmethyl)-1H-indole-4-carboxylate was prepared using the general procedure for Suzuki coupling from **120** (50 mg, 0.145 mmol, 1.0 equiv). Purification by flash chromatography (hexanes/EtOAc gradient) afforded the methyl ester of the title compound (59 mg, 63%) as a white solid: R_f 0.30 (EtOAc); ^1H NMR (600 MHz, CDCl_3) δ 4.02 (s, 3H), 5.42 (s, 2H), 6.95 (d, J = 6.0 Hz, 2H), 7.25 (d, J = 3.0 Hz, 1H), 7.29 (d, J = 3.0 Hz, 1H), 7.33 (t, J = 7.2 Hz, 1H), 7.43 (t, J = 7.2 Hz, 2H), 7.55 (s, 1H), 7.58 (d, J = 7.2 Hz, 2H), 8.21 (s, 1H), 8.53 (d, J = 6.0 Hz, 2H); ^{13}C NMR (150 MHz, CDCl_3) δ 49.3, 52.0, 103.9, 112.5, 121.3, 122.5, 123.4, 127.3, 127.5, 127.7, 129.0, 131.0, 135.4, 137.7, 141.2, 146.3, 150.5, 167.9.

Methyl 6-phenyl-1-(pyridin-4-ylmethyl)-1H-indole-4-carboxylate (50 mg, 0.146 mmol, 1.0 equiv) prepared above was converted to the title compound using the general procedure for ester hydrolysis. Purification by preparative reverse-phase HPLC using method 7 afforded the title compound (9.4 mg, 20%) as a white solid: R_T 14.5 min; ^1H NMR (600 MHz, DMSO- d_6) δ 5.54 (s, 2H), 7.07 (d, J = 6.0 Hz, 2H), 7.19 (d, J = 3.0 Hz, 1H), 7.27 (d, J = 3.0 Hz, 1H), 7.33 (t, J = 7.2 Hz, 1H), 7.39–7.43 (m, 3H), 7.64 (d, J = 7.2 Hz, 2H), 7.90 (s, 1H), 8.44 (d, J = 6.0 Hz, 2H); ^{13}C NMR (150 MHz, DMSO- d_6) δ 48.1, 104.5, 108.3, 120.7, 121.9, 126.6, 126.9, 128.0, 129.0, 129.6, 133.0, 137.4, 141.9, 148.0, 149.9, 157.0, 170.8; HRMS (ESI $^-$) calcd for $\text{C}_{21}\text{H}_{15}\text{N}_2\text{O}_2$ [M - H] $^-$ 327.1139, found 327.1145 (error 1.8 ppm).

Enzyme Binding Studies: BasE and MbtA were expressed in *E. coli* and purified as described.^{38, 39} Determination of equilibrium dissociation constants K_D for each compound was performed using the fluorescence polarization assay with Fl-Sal-AMS **14** as ligand in black flat bottom 96-well plates (Costar #3915) as described.³⁹ A three-fold serial dilution of each compound (10 μL) was added to 90 μL of a solution of **14** (20 nM final concentration) and 200 nM BasE or 50 nM MbtA, in 30 mM Tris-HCl pH 7.5, 1 mM MgCl_2 and 0.0025% Igepal CA-630. The fluorescence anisotropy was measured after a 30 min incubation at 25 $^\circ\text{C}$. The K_D 's of each compound tested were determined by fitting the displacement curves (A_{OBS} , the experimentally measured anisotropy vs. L_T , the test compound concentration) to Equations 1 and 2⁴⁶ using Mathematica 7 (Wolfram Research Inc.). In these equations, Q is the ratio of the fluorescence intensity of the probe in the bound and free states (1.07 for BasE and 1.02 for MbtA³⁹), F_{SB} is the fraction of bound **14**, A_B (0.035) and A_F (0.220 for BasE and 0.308 for MbtA³⁹), represent the anisotropies of bound and free probe **14**, K_{D1} is the equilibrium dissociation constant of **14** (84.3 nM for BasE and

9.26 nM for MbtA³⁹), L_{ST} is the concentration of **14**, R_T is the receptor protein concentration and K_{D2} is the test compound's equilibrium dissociation constant.⁴⁶

$$A_{OBS} = \frac{QF_{SB}A_B + (1-F_{SB})A_F}{1 - (1-Q)F_{SB}} \quad (1)$$

$$F_{SB} = \frac{2\sqrt{(a^2-3b)}\cos(\theta/3) - a}{3K_{D1} + 2\sqrt{(a^2-3b)}\cos(\theta/3) - a} \quad (2)$$

with

$$\begin{aligned} a &= K_{D1} + K_{D2} + L_{ST} + L_T - R_T \\ b &= (L_T - R_T)K_{D1} + (L_{ST} - R_T)K_{D2} + K_{D1}K_{D2} \\ c &= -K_{D1}K_{D2}R_T \\ \theta &= \arccos \left[\frac{-2a^3 + 9ab - 27c}{2\sqrt{(a^2-3b)^3}} \right] \end{aligned}$$

***Acinetobacter baumannii* MIC Assay:** A single LB agar plate was streaked with 19606 WT and grown overnight at 30° C. The plate was flooded with 2 mL of medium 1 (M9 minimal media, 0.2% casamino acids, 200 μM dipyriddy) and transferred to a 15 mL centrifuge tube. Cells were spun down at room temperature and washed twice with 10 mL medium 1 and then resuspended in 2 mL medium 1. The A_{600} was measured and cells were diluted in medium 1 to an A_{600} of 1.7 – 2.0 and then further diluted to 0.0003 in either medium 1 supplemented with 1 μM FeCl₃ or Medium 2 (M9 minimal media, 0.2% casamino acids) supplemented with 200 μM FeCl₃ and 200 μL of each solution was dispensed in triplicate into a 96 well plate containing 2 μL of each inhibitor in DMSO for a final concentration of 100 μM. Tetracycline was used as a positive control (100 ng/mL) and 1% DMSO was used as a negative control. The plates were incubated at 30° C and the A_{600} was measured at 15 hours.

***Mycobacterium tuberculosis H37RV* MIC Assay:** Minimum inhibitory concentrations (MICs) were experimentally determined as previously described.³⁶ MICs were determined in quadruplicate in iron-deficient GAST and GAST supplemented with 200 μM FeCl₃ according to the broth microdilution method using compounds from DMSO stock solutions or with control wells treated with an equivalent amount of DMSO. Isoniazid was used as a positive control while DMSO was employed as a negative control. All measurements reported herein used an initial cell density of 10⁴–10⁵ cells/assay and growth was monitored at 10–14 days, with the untreated and DMSO-treated control cultures reaching an OD₆₂₀ 0.2–0.3. Plates were incubated at 37 °C (100 μL/well) and growth was recorded by measurement of optical density at 620 nm.

Protein Crystallography: The BasE enzyme from *A. baumannii* strain AB900 for crystallographic studies was produced and crystallized as described.³¹ BasE was co-crystallized with **67** and **70**; crystals were isomorphous with the prior BasE structures. Data were collected at SSRL beamline 11-1. Initial phases were provided by difference Fourier methods using the previous structure of BasE bound to **15** as an initial refinement model; all non-protein atoms were removed prior to refinement. The models were refined to completion as described previously.³¹

Insertional deletion of *BasE*: Flanking regions of *basE* from *A. baumannii* ATCC 19606 were amplified by PCR using the primers 5' F, 5' R (CACCGAGCTCGGATCCACTGGATGTGGTGAGAAGC, CCCGGGACTAGTGACATTCTAAATATTCAATTTAATTTAATG) and 3' F, 3' R (CACCCGGGCTAGCTAAATATTGAGCAGCATATGG, CCTGCAGGATCCATGTGCTCTGAAGGACACG). The kanamycin resistance gene (*kanR*) was amplified from pCR2.1 TOPO (Invitrogen) using the primers Kan F, Kan R (CACCCTAGTTAACCGGAATTGCCAGCTGGG, GCTAGCTCAGAAGAAGACTCGTCAAG). The three PCR fragments were cloned into pENTR/TEV/D-TOPO (Invitrogen) for ease of propagation creating pCDD129, pCDD130 and pCDD131 for the 5', KanR, and 3' fragments respectively. The knockout fragments were cloned sequentially into pUC18 by first ligating the 5' fragment after digesting pCDD129 and pUC18 with *SacI* and *SmaI* creating pCDD132. The 3' fragment was added next by ligating *SmaI*, *SbfI* digested pCDD131 and pCDD132, creating pCDD133. KanR was removed from pCDD130 by digestion with *SpeI*, *NheI* and ligated into similarly cut pCDD133 creating pCDD134. The knock out cassette was removed from pCDD134 by digestion with *BamHI* and cloned into pKC1139 a *Streptomyces/E. coli* shuttle vector to create pCDD135, which will act as a suicide vector in *A. baumannii*. The knock out plasmid was transformed into ATCC 19606 using electroporation as previously described.^{64, 65} Clones resistant to kanamycin and sensitive to apramycin were confirmed by PCR to have the correct genome insertion using the primer pairs 5' confirm (CACACGAGGTATTTTGTGCTGGG), KanR, and KanF, 3' confirm (CACACGAGGTATTTTGTGCTGGG), creating 19606 Δ *basE*.

Complementation of 19606 Δ *basE*: The *E. coli*, *A. baumannii* shuttle vector pWH1266 (ATCC, Manassas VA) was used to complement 19606 Δ *basE*. The primers *basE* comp F (CACCGGATCCTTGTTAATCATTTCGAATTTTG), and *basE* comp R (GCATGCTTAAGATGTTGTAGATGTATTTAAAATGC) were used to PCR amplify *basE* and its promoter region from ATCC19606. Primers Apr F (CACCAAGCTTTAAGGTTTCATGTGCAGCTCCATC) and Apr R (GGATCCTCAGCCAATCGACTGGCG) were used to amplify the apramycin resistance (*aprR*) gene from pKC1139. The *basE* fragment was digested with *BamHI* and *SphI*, and AprR was digested with *BamHI* and *HindIII*. Both fragments were ligated into pWH1266 digested with *HindIII* and *SphI* creating pCDD140. The final plasmid was transformed into 19606 Δ *basE* using the method described above.

Growth of *A. baumannii* strains: LB agar plates were streaked with 19606 WT, 19606 Δ *basE*, or 19606 Δ *basE* pCDD140 and grown overnight at 30° C. Each plate was flooded with 2 mL of medium 1 (M9 minimal media, 0.2% casamino acids, 200 μ M dipyrityl) and transferred to a 15 mL centrifuge tube. Cells were spun down at rt and washed twice with 10 mL medium 1 and then resuspended in 2 mL medium 1. The A_{600} was measured and cells were diluted in medium 1 to an A_{600} of 1.7–2.0 and then further diluted to 0.0003 in either medium 1 supplemented with 1 μ M FeCl₃ or Medium 2 (M9 minimal media, 0.2% casamino acids) supplemented with 200 μ M FeCl₃ and placed into a 96 well plate in six 200 μ L replicates. Positive controls for iron limiting and rich conditions consisted of WT supplemented with 100 ng/mL tetracycline. The plates were incubated at 30° C and the A_{600} was measured at 2, 4, 6, 7, 8, 9, 10, 12, 13 and 22 h.

Supplementary Material

Refer to Web version on PubMed Central for supplementary material.

Acknowledgments

This research was supported by grants from the National Institutes of Health (AI070219 to C.C.A. and GM-068440 to A.M.G.) and the Intramural Research Program of the NIAID in the National Institutes of Health (to Clifton E. Barry 3rd). We thank Dr. Michael Walters (Institute for Therapeutics Discovery and Development, University of Minnesota) for assistance with the parallel synthesis and Prof. David H. Sherman (Life Sciences Institute, University of Michigan) for plasmids pUC18 and pKC1139.

Abbreviations

AAAE	aryl acid adenylating enzyme
ArCP	aryl carrier protein
BOP	(benzotriazol-1-yloxy)tris(dimethylamino)phosphonium hexafluorophosphate
DHB	2,3-dihydroxybenzoic acid
DHB-AMS	5'- <i>O</i> -[<i>N</i> -(2,3-dihydroxybenzoyl)sulfamoyl]adenosine
Fl-Sal-AMS	22- <i>O</i> -{2-[2-(2-[(fluorescein-5-yl)carbonyl]amino)ethoxy)ethoxy]ethoxy}-52- <i>O</i> -[<i>N</i> -(salicyl)sulfamoyl]adenosine
FP	fluorescence polarization
HPLC	high-performance liquid chromatography
HTS	high-throughput screening
MDR	multidrug resistant
MIC	minimum inhibitory concentration
NRPS	nonribosomal peptide synthetase
PMP	<i>p</i> -methoxyphenyl
PyBroP	bromotripyrrolidinophosphonium hexafluorophosphate
ROS	reactive oxygen species
SAL	salicylic acid
Sal-AMS	5'- <i>O</i> -[<i>N</i> -(salicyl)sulfamoyl]adenosine
SAR	structure–activity relationship
TES	triethylsilyl
TFA	trifluoroacetic acid

References

1. Projan SJ, Bradford PA. Late stage antibacterial drugs in the clinical pipeline. *Curr Opin Microbiol.* 2007; 10:441–446. [PubMed: 17950658]
2. Wright GD. Antibiotics: a new hope. *Chem Biol.* 2012; 19:3–10. [PubMed: 22284349]
3. Peleg AY, Seifert H, Paterson DL. *Acinetobacter baumannii*: emergence of a successful pathogen. *Clin Microbiol Rev.* 2008; 21:538–582. [PubMed: 18625687]
4. Calhoun JH, Murray CK, Manring MM. Multidrug-resistant organisms in military wounds from Iraq and Afghanistan. *Clin Orthop Relat Res.* 2008; 466:1356–1362. [PubMed: 18347888]
5. Lockhart SR, Abramson MA, Beekmann SE, Gallagher G, Riedel S, Diekema DJ, Quinn JP, Doern GV. Antimicrobial resistance among Gram-negative bacilli causing infections in intensive care unit

- patients in the United States between 1993 and 2004. *J Clin Microbiol.* 2007; 45:3352–3359. [PubMed: 17715376]
6. Rhomberg PR, Jones RN. Summary trends for the Meropenem Yearly Susceptibility Test Information Collection Program: a 10-year experience in the United States (1999–2008). *Diagn Microbiol Infect Dis.* 2009; 65:414–426. [PubMed: 19833471]
 7. Vallenet D, Nordmann P, Barbe V, Poirel L, Mangenot S, Bataille E, Dossat C, Gas S, Kreimeyer A, Lenoble P, Oztas S, Poulain J, Segurens B, Robert C, Abergel C, Claverie JM, Raoult D, Medigue C, Weissenbach J, Cruveiller S. Comparative analysis of *Acinetobacter* genomes for three lifestyles. *PLoS ONE.* 2008; 3:e1805. [PubMed: 18350144]
 8. Adams MD, Goglin K, Molyneaux N, Hujer KM, Lavender H, Jamison JJ, MacDonald IJ, Martin KM, Russo T, Campagnari AA, Hujer AM, Bonomo RA, Gill SR. Comparative genome sequence analysis of multidrug-resistant *Acinetobacter baumannii*. *J Bacteriol.* 2008; 190:8053–8064. [PubMed: 18931120]
 9. Falagas ME, Kasiakou SK. Colistin: the revival of polymyxins for the management of multidrug-resistant gram-negative bacterial infections. *Clin Infect Dis.* 2005; 40:1333–1341. [PubMed: 15825037]
 10. Cai Y, Chai D, Wang R, Liang B, Bai N. Colistin resistance of *Acinetobacter baumannii*: clinical reports, mechanisms and antimicrobial strategies. *J Antimicrob Chemother.* 2012; 67:1607–1615. [PubMed: 22441575]
 11. Posey JE, Gherardini FC. Lack of a role for iron in the Lyme disease pathogen. *Science.* 2000; 288:1651–1653. [PubMed: 10834845]
 12. Miethke M, Marahiel MA. Siderophore-based iron acquisition and pathogen control. *Microbiol Mol Biol Rev.* 2007; 71:413–451. [PubMed: 17804665]
 13. Crosa JH, Walsh CT. Genetics and assembly line enzymology of siderophore biosynthesis in bacteria. *Microbiol Mol Biol Rev.* 2002; 66:223–249. [PubMed: 12040125]
 14. Sandy M, Butler A. Microbial iron acquisition: marine and terrestrial siderophores. *Chem Rev.* 2009; 109:4580–4595. [PubMed: 19772347]
 15. Hider RC, Kong X. Chemistry and biology of siderophores. *Nat Prod Rep.* 2010; 27:637–657. [PubMed: 20376388]
 16. Zimble DL, Penwell WF, Gaddy JA, Menke SM, Tomaras AP, Connerly PL, Actis LA. Iron acquisition functions expressed by the human pathogen *Acinetobacter baumannii*. *Biometals.* 2009; 22:23–32. [PubMed: 19130255]
 17. Lawlor MS, O'Connor C, Miller VL. Yersiniabactin is a virulence factor for *Klebsiella pneumoniae* during pulmonary infection. *Infect Immun.* 2007; 75:1463–1472. [PubMed: 17220312]
 18. Takase H, Nitanai H, Hoshino K, Otani T. Impact of siderophore production on *Pseudomonas aeruginosa* infections in immunosuppressed mice. *Infect Immun.* 2000; 68:1834–1839. [PubMed: 10722571]
 19. Fischbach MA, Lin H, Zhou L, Yu Y, Abergel RJ, Liu DR, Raymond KN, Wanner BL, Strong RK, Walsh CT, Aderem A, Smith KD. The pathogen-associated *iroA* gene cluster mediates bacterial evasion of lipocalin 2. *Proc Natl Acad Sci USA.* 2006; 103:16502–16507. [PubMed: 17060628]
 20. Cendrowski S, MacArthur W, Hanna P. *Bacillus anthracis* requires siderophore biosynthesis for growth in macrophages and mouse virulence. *Mol Microbiol.* 2004; 51:407–417. [PubMed: 14756782]
 21. Dale SE, Doherty-Kirby A, Lajoie G, Heinrichs DE. Role of siderophore biosynthesis in virulence of *Staphylococcus aureus*: identification and characterization of genes involved in production of a siderophore. *Infect Immun.* 2004; 72:29–37. [PubMed: 14688077]
 22. De Voss JJ, Rutter K, Schroeder BG, Su H, Zhu Y, Barry CE 3rd. The salicylate-derived mycobactin siderophores of *Mycobacterium tuberculosis* are essential for growth in macrophages. *Proc Natl Acad Sci USA.* 2000; 97:1252–1257. [PubMed: 10655517]
 23. Kohanski MA, Dwyer DJ, Hayete B, Lawrence CA, Collins JJ. A common mechanism of cellular death induced by bactericidal antibiotics. *Cell.* 2007; 130:797–810. [PubMed: 17803904]
 24. Dwyer DJ, Kohanski MA, Collins JJ. Role of reactive oxygen species in antibiotic action and resistance. *Curr Opin Microbiol.* 2009; 12:482–489. [PubMed: 19647477]

25. Yamamoto S, Okujo N, Sakakibara Y. Isolation and structure elucidation of acinetobactin, a novel siderophore from *Acinetobacter baumannii*. Arch Microbiol. 1994; 162:249–254. [PubMed: 7802543]
26. Takeuchi Y, Ozaki S, Satoh M, Mimura K, Hara S, Abe H, Nishioka H, Harayama T. Synthesis of acinetobactin. Chem Pharm Bull (Tokyo). 2010; 58:1552–1553. [PubMed: 21048355]
27. Dorsey CW, Tomaras AP, Connerly PL, Tolmasky ME, Crosa JH, Actis LA. The siderophore-mediated iron acquisition systems of *Acinetobacter baumannii* ATCC 19606 and *Vibrio anguillarum* 775 are structurally and functionally related. Microbiology. 2004; 150:3657–3667. [PubMed: 15528653]
28. Mihara K, Tanabe T, Yamakawa Y, Funahashi T, Nakao H, Narimatsu S, Yamamoto S. Identification and transcriptional organization of a gene cluster involved in biosynthesis and transport of acinetobactin, a siderophore produced by *Acinetobacter baumannii* ATCC 19606T. Microbiology. 2004; 150:2587–2597. [PubMed: 15289555]
29. Sattely ES, Walsh CT. A latent oxazoline electrophile for N-O-C bond formation in pseudomonine biosynthesis. J Am Chem Soc. 2008; 130:12282–12284. [PubMed: 18710233]
30. Wuest WM, Sattely ES, Walsh CT. Three siderophores from one bacterial enzymatic assembly line. J Am Chem Soc. 2009; 131:5056–5057. [PubMed: 19320483]
31. Drake EJ, Duckworth BP, Neres J, Aldrich CC, Gulick AM. Biochemical and structural characterization of bisubstrate inhibitors of BasE, the self-standing nonribosomal peptide synthetase adenylate-forming enzyme of acinetobactin synthesis. Biochemistry. 2010; 49:9292–9305. [PubMed: 20853905]
32. Hurdle JG, O’Neill AJ, Chopra I. Prospects for aminoacyl-tRNA synthetase inhibitors as new antimicrobial agents. Antimicrob Agents Chemother. 2005; 49:4821–4833. [PubMed: 16304142]
33. Sikora AL, Wilson DJ, Aldrich CC, Blanchard JS. Kinetic and inhibition studies of dihydroxybenzoate-AMP ligase from *Escherichia coli*. Biochemistry. 2010; 49:3648–3657. [PubMed: 20359185]
34. Gulick AM. Conformational dynamics in the Acyl-CoA synthetases, adenylation domains of non-ribosomal peptide synthetases, and firefly luciferase. ACS Chem Biol. 2009; 4:811–827. [PubMed: 19610673]
35. Ferreras JA, Ryu JS, Di Lello F, Tan DS, Quadri LE. Small-molecule inhibition of siderophore biosynthesis in *Mycobacterium tuberculosis* and *Yersinia pestis*. Nat Chem Biol. 2005; 1:29–32. [PubMed: 16407990]
36. Somu RV, Boshoff H, Qiao CH, Bennett EM, Barry CE, Aldrich CC. Rationally designed nucleoside antibiotics that inhibit siderophore biosynthesis of *Mycobacterium tuberculosis*. J Med Chem. 2006; 49:31–34. [PubMed: 16392788]
37. Miethke M, Bissleret P, Beckering CL, Vignard D, Eustache J, Marahiel MA. Inhibition of aryl acid adenylation domains involved in bacterial siderophore synthesis. FEBS J. 2006; 273:409–419. [PubMed: 16403027]
38. Somu RV, Wilson DJ, Bennett EM, Boshoff HI, Celia L, Beck BJ, Barry CE, Aldrich CC. Antitubercular nucleosides that inhibit siderophore biosynthesis: SAR of the glycosyl domain. J Med Chem. 2006; 49:7623–7635. [PubMed: 17181146]
39. Neres J, Wilson DJ, Celia L, Beck BJ, Aldrich CC. Aryl acid adenylating enzymes involved in siderophore biosynthesis: Fluorescence polarization assay, ligand specificity, and discovery of non-nucleoside inhibitors via high-throughput screening. Biochemistry. 2008; 47:11735–11749. [PubMed: 18928302]
40. Hohn H. Ein neues Verfahren zur Darstellung von 5-Amino-pyrazolen. Z Chem. 1970; 10:386–388.
41. Dorn H, Müller T. Zur direkten (C-4)-Substitution von Amino-pyrazolen mit β -Keto-carbonyl-Verbindungen — 1-Benzyl-6, 7-dihydro-4-ethoxycarbonyl-6-oxo-pyrazolo[3,4-*b*]pyridin. Z Chem. 1980; 20:95.
42. Kang FA, Sui ZH, Murray WV. Pd-catalyzed direct arylation of tautomerizable heterocycles with aryl boronic acids via C-OH bond activation using phosphonium salts. J Am Chem Soc. 2008; 130:11300–11302. [PubMed: 18665598]

43. Wan ZK, Wacharasindhu S, Levins CG, Lin M, Tabei K, Mansour TS. The scope and mechanism of phosphonium-mediated S(N)Ar reactions in heterocyclic amides and ureas. *J Org Chem.* 2007; 72:10194–10210. [PubMed: 18044930]
44. Gupte A, Boshoff HI, Wilson DJ, Neres J, Labello NP, Somu RV, Xing C, Barry CE, Aldrich CC. Inhibition of siderophore biosynthesis by 2-triazole substituted analogues of 5'-O-[N-(salicyl)sulfamoyl]adenosine: antibacterial nucleosides effective against *Mycobacterium tuberculosis*. *J Med Chem.* 2008; 51:7495–7507. [PubMed: 19053762]
45. Shi C, Aldrich CC. Efficient Pd-catalyzed coupling of tautomerizable heterocycles with terminal alkynes via C-OH bond activation using PyBroP. *Org Lett.* 2010; 12:2286–2289. [PubMed: 20411949]
46. Roehrl MHA, Wang JY, Wagner G. A general framework for development and data analysis of competitive high-throughput screens for small-molecule inhibitors of protein - Protein interactions by fluorescence polarization. *Biochemistry.* 2004; 43:16056–16066. [PubMed: 15610000]
47. Stachelhaus T, Mootz HD, Marahiel MA. The specificity-conferring code of adenylation domains in nonribosomal peptide synthetases. *Chem Biol.* 1999; 6:493–505. [PubMed: 10421756]
48. Auld DS, Lovell S, Thorne N, Lea WA, Maloney DJ, Shen M, Rai G, Battaile KP, Thomas CJ, Simeonov A, Hanzlik RP, Ingles J. Molecular basis for the high-affinity binding and stabilization of firefly luciferase by PTC124. *Proc Natl Acad Sci USA.* 2010; 107:4878–4883. [PubMed: 20194791]
49. Lee TV, Johnson LJ, Johnson RD, Koulman A, Lane GA, Lott JS, Arcus VL. Structure of a eukaryotic nonribosomal peptide synthetase adenylation domain that activates a large hydroxamate amino acid in siderophore biosynthesis. *J Biol Chem.* 2010; 285:2415–2427. [PubMed: 19923209]
50. Gordon NC, Wareham DW. Multidrug-resistant *Acinetobacter baumannii*: mechanisms of virulence and resistance. *Int J Antimicrob Agents.* 2010; 35:219–226. [PubMed: 20047818]
51. Quadri LE. Strategic paradigm shifts in the antimicrobial drug discovery process of the 21st century. *Infect Disord Drug Targets.* 2007; 7:230–237. [PubMed: 17897059]
52. Frederick RE, Mayfield JA, DuBois JL. Iron trafficking as an antimicrobial target. *Biometals.* 2009; 22:583–593. [PubMed: 19350396]
53. Ballouche M, Cornelis P, Baysse C. Iron metabolism: a promising target for antibacterial strategies. *Recent Pat Antiinfect Drug Discov.* 2009; 4:190–205. [PubMed: 19594436]
54. Cescau S, Cwerman H, Letoffe S, Delepeleire P, Wandersman C, Biville F. Heme acquisition by hemophores. *Biometals.* 2007; 20:603–613. [PubMed: 17268821]
55. Budzikiewicz, H. *Microbial Siderophores*. Vol. 92. Springer-Verlag; Wien: 2010. p. 75
56. Fischbach MA, Walsh CT. Antibiotics for emerging pathogens. *Science.* 2009; 325:1089–1093. [PubMed: 19713519]
57. Adler C, Corbalan NS, Seyedsayamdost MR, Pomares MF, de Cristobal RE, Clardy J, Kolter R, Vincent PA. Catecholate siderophores protect bacteria from pyochelin toxicity. *PLoS One.* 2012; 7:e46754. [PubMed: 23071628]
58. Dorsey CW, Tolmasky ME, Crosa JH, Actis LA. Genetic organization of an *Acinetobacter baumannii* chromosomal region harbouring genes related to siderophore biosynthesis and transport. *Microbiology.* 2003; 149:1227–1238. [PubMed: 12724384]
59. Penwell WF, Arivett BA, Actis LA. The *Acinetobacter baumannii* entA gene located outside the acinetobactin cluster is critical for siderophore production, iron acquisition and virulence. *PLoS One.* 2012; 7:e36493. [PubMed: 22570720]
60. Gaddy JA, Arivett BA, McConnell MJ, Lopez-Rojas R, Pachon J, Actis LA. Role of acinetobactin-mediated iron acquisition functions in the interaction of *Acinetobacter baumannii* strain ATCC 19606T with human lung epithelial cells, *Galleria mellonella* caterpillars, and mice. *Infect Immun.* 2012; 80:1015–1024. [PubMed: 22232188]
61. Eijkelkamp BA, Hassan KA, Paulsen IT, Brown MH. Investigation of the human pathogen *Acinetobacter baumannii* under iron limiting conditions. *BMC Genomics.* 2011; 12:126. [PubMed: 21342532]
62. Antunes LC, Imperi F, Towner KJ, Visca P. Genome-assisted identification of putative iron-utilization genes in *Acinetobacter baumannii* and their distribution among a genotypically diverse collection of clinical isolates. *Res Microbiol.* 2011; 162:279–284. [PubMed: 21144895]

63. Misra RN, Rawlins DB, Xiao HY, Shan WF, Bursuker I, Kellar KA, Mulheron JG, Sack JS, Tokarski JS, Kimball SD, Webster KR. 1*H*-pyrazolo[3,4-*b*]pyridine inhibitors of cyclin-dependent kinases. *Bioorg Med Chem Lett*. 2003; 13:1133–1136. [PubMed: 12643928]
64. Higgins PG, Poirel L, Lehmann M, Nordmann P, Seifert H. OXA-143, a novel carbapenem-hydrolyzing class D beta-lactamase in *Acinetobacter baumannii*. *Antimicrob Agents Chemother*. 2009; 53:5035–5038. [PubMed: 19770279]
65. Choi KH, Kumar A, Schweizer HP. A 10-min method for preparation of highly electrocompetent *Pseudomonas aeruginosa* cells: application for DNA fragment transfer between chromosomes and plasmid transformation. *J Microbiol Methods*. 2006; 64:391–397. [PubMed: 15987659]

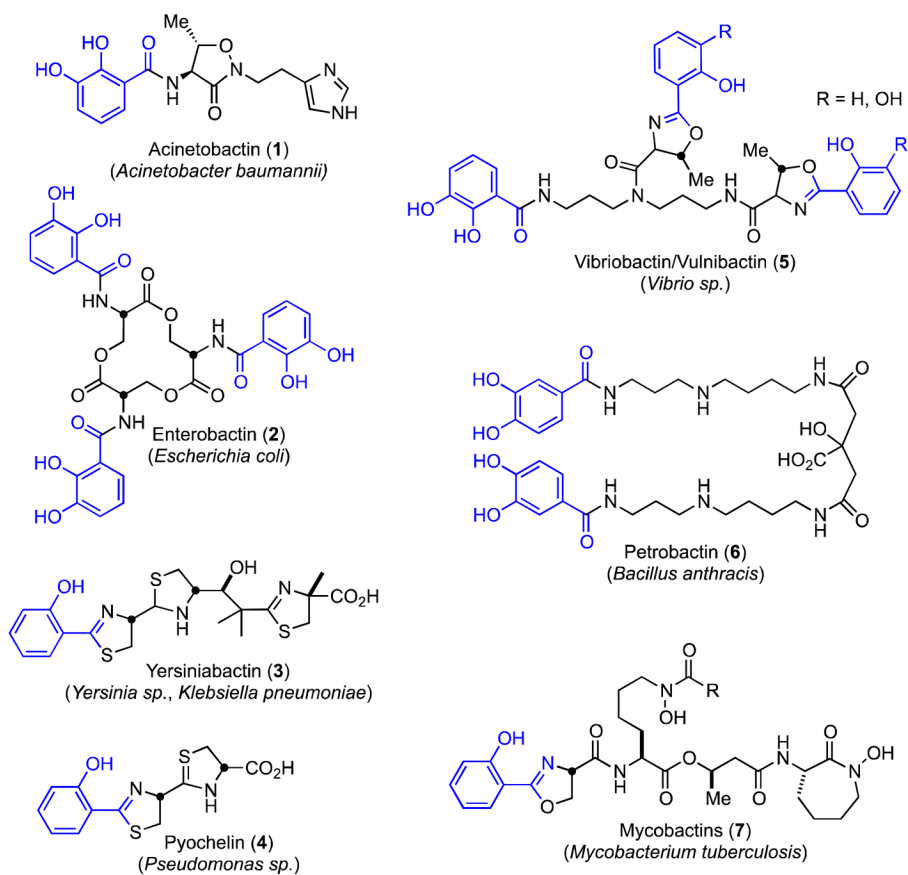


Figure 1.
Structure of representative aryl-capped siderophores

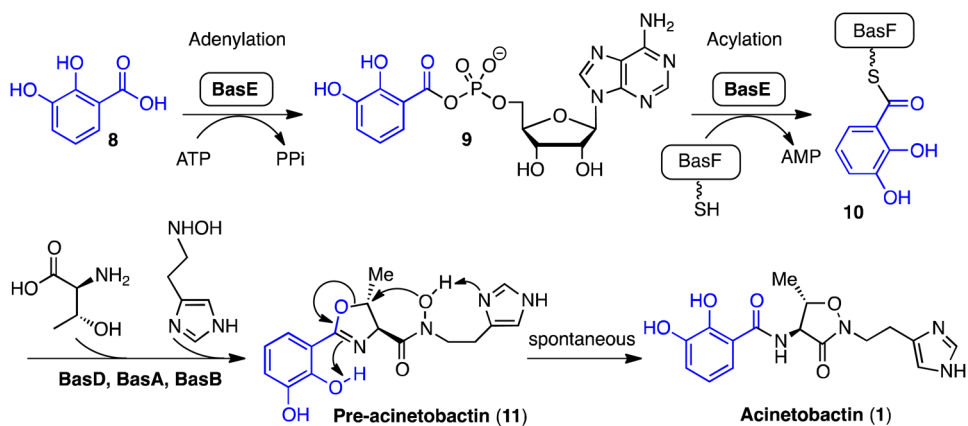


Figure 2. Biosynthesis of Acinetobactin

BasE binds 2,3-dihydroxybenzoic acid **8** and ATP then catalyzes their condensation to form an intermediate acyl-adenylate **9** that remains tightly bound. In a second half reaction, BasE catalyzes the transfer of the acyl group (blue) onto a nucleophilic sulfur atom of the aryl carrier domain of BasF to provide the acylated complex **10** with the release of AMP. Further steps are catalyzed by BasD, BasA and BasB, incorporating threonine and *N*-hydroxyhistamine to yield pre-acinetobactin **11**. This molecule undergoes a facile rearrangement to the isoxazolidinone isomer of acinetobactin **1** that is likely promoted via an internal hydrogen bond with the oxazoline nitrogen atom in conjunction with the proximal imidazole moiety that serves to deprotonate the *N*-hydroxyamide functional group.

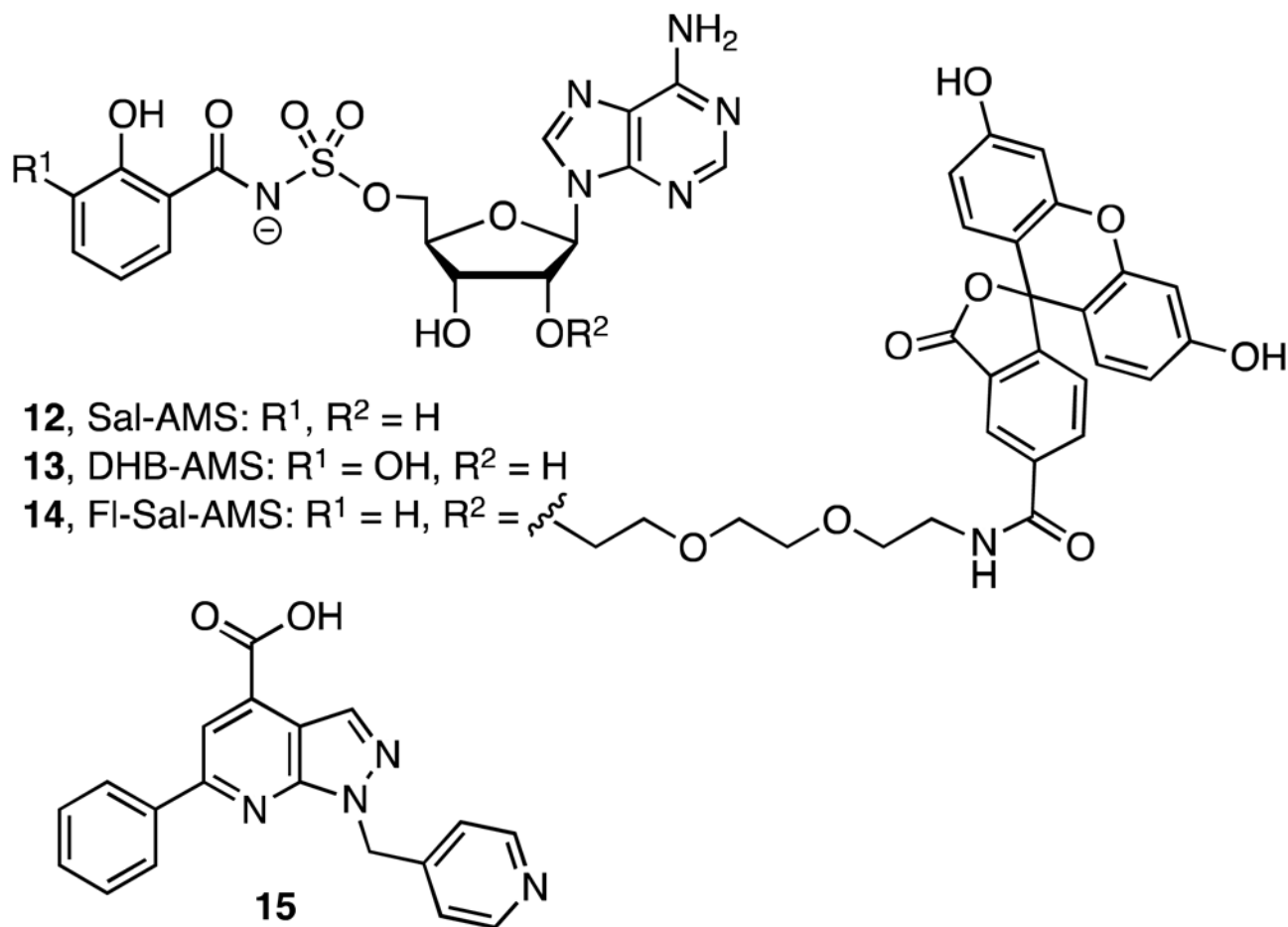


Figure 3. Inhibitor and probe structures. 5'-*O*-[*N*-(salicyl)sulfamoyl]adenosine (Sal-AMS, **12**), 5'-*O*-[*N*-(2,3-dihydroxybenzoyl)sulfamoyl]adenosine (2,3-DHB-AMS, **13**), fluorescent probe **14**, and HTS hit 6-phenyl-1-(pyridin-4-ylmethyl)-1*H*-pyrazolo[3,4-*b*]pyridine-4-carboxylic acid (**15**).

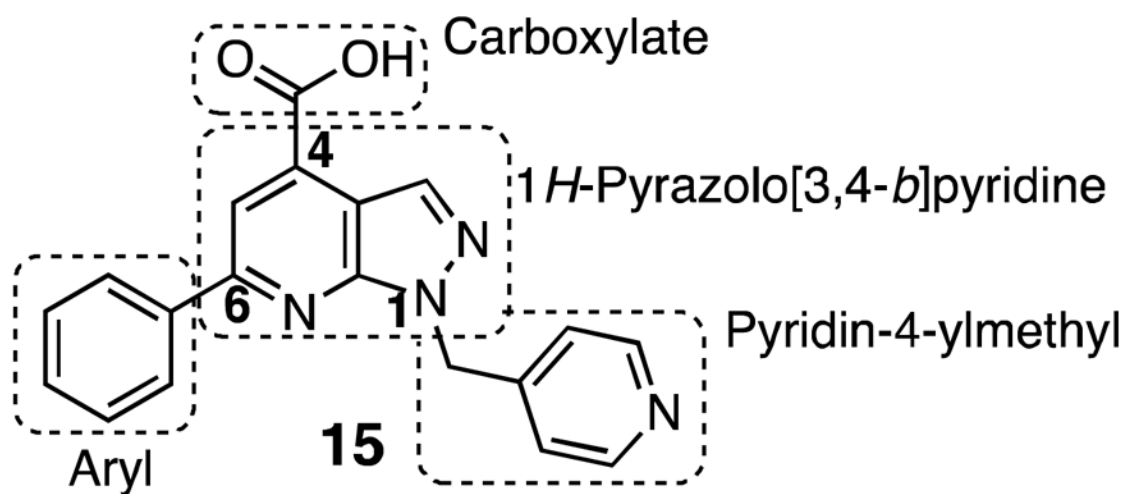


Figure 4. Dissection of pyrazolopyridine hit **15** into 4 domains for SAR analysis.

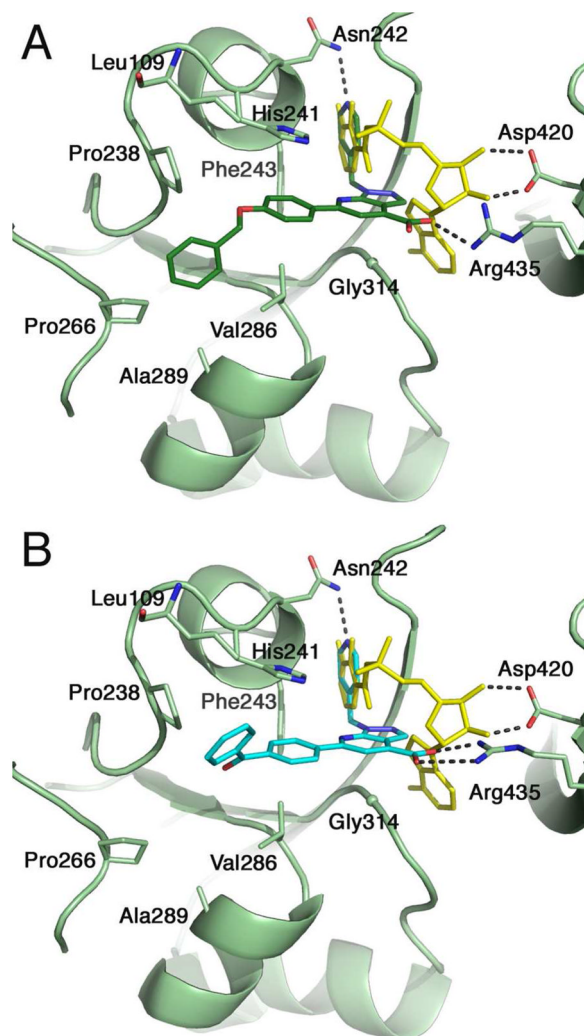


Figure 5. Structural characterization of inhibitor binding. Ribbon diagrams are shown for the BasE enzyme bound to A. Inhibitor **67** and B. Inhibitor **70**. Superimposed on both panels is the nucleotide DHB-AMS **13** (yellow) from PDB 3O82, demonstrating the interaction between Asp420 and the ribose hydroxyls and how the pyridyl group of the inhibitors mimics DHB moiety. Arg435, which is weakly ordered in both chains, interacts with the inhibitor carboxylate. Residues that form the hydrophobic binding pocket are shown in side chain representation.

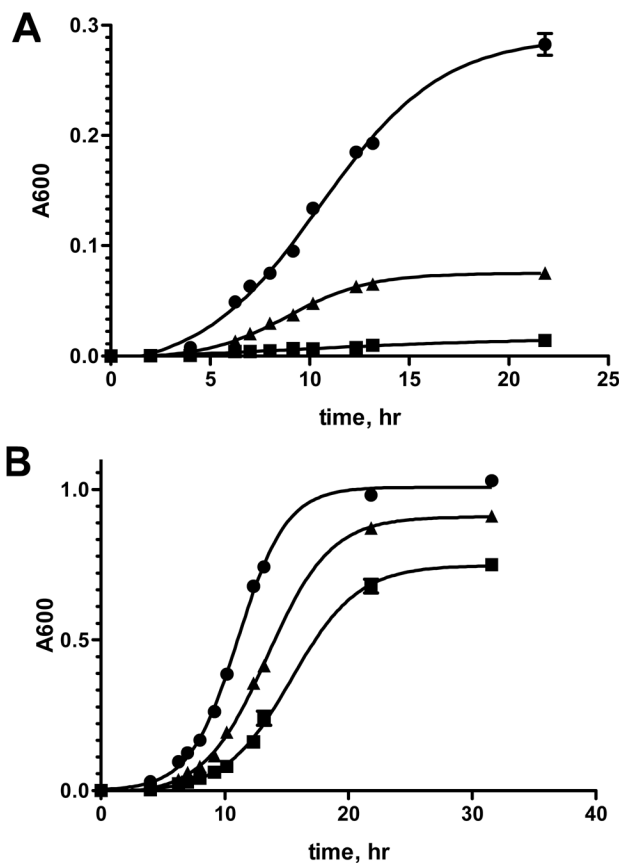
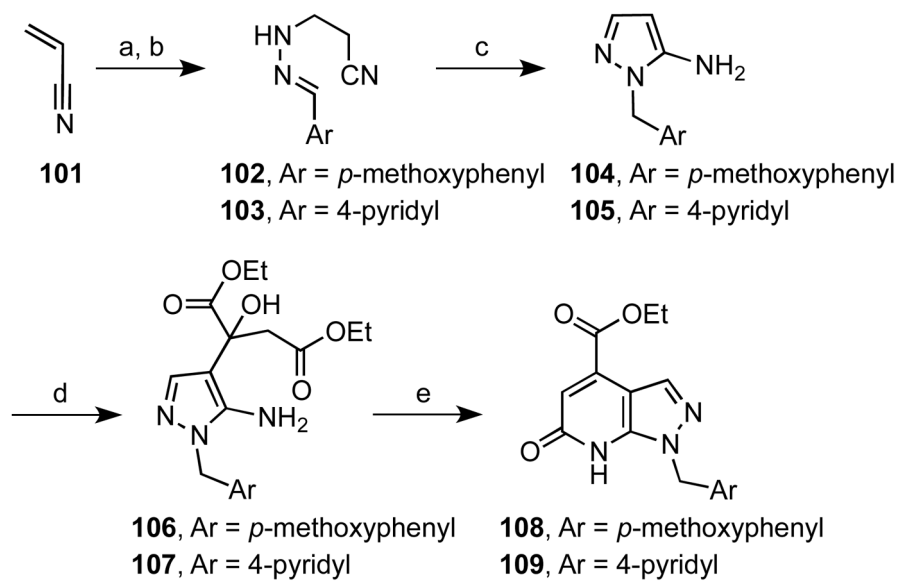
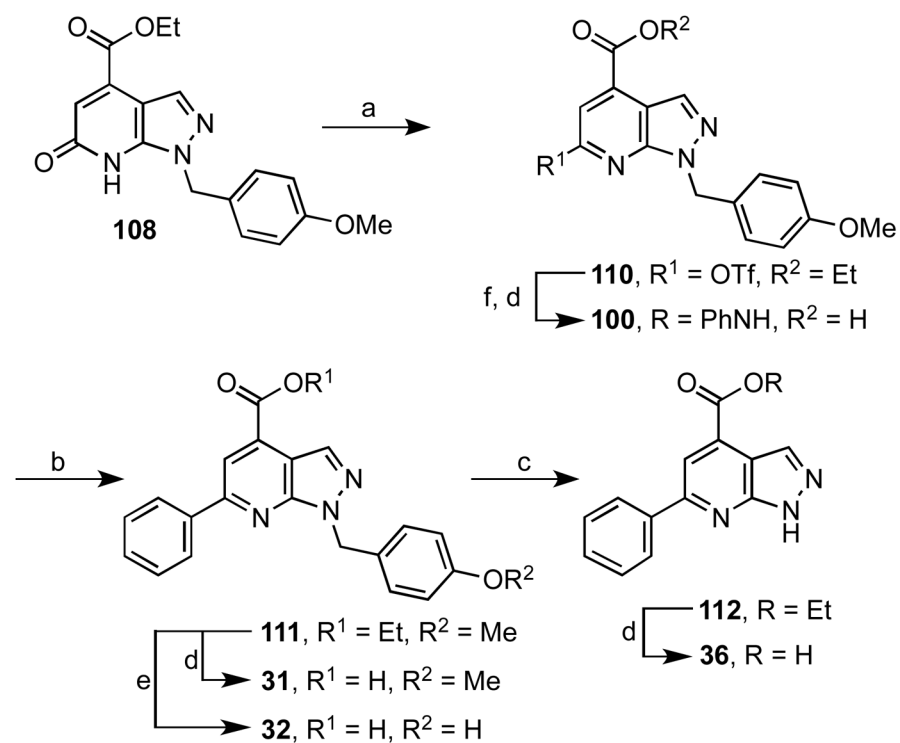


Figure 6.

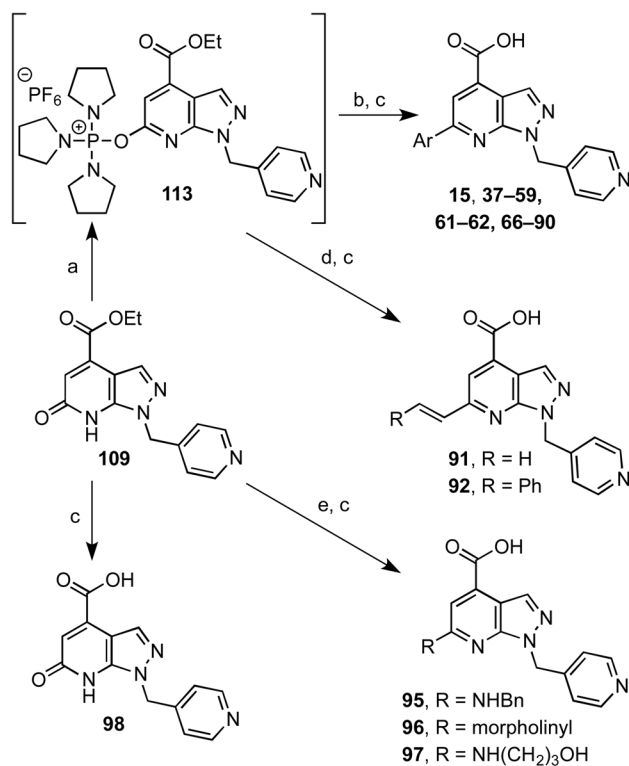
In vitro growth curves of wild type *A. baumannii* ATCC 19606 (●), Δ *basE::kan* mutant (■), and the Δ *basE::kan* mutant complemented with plasmid pCDD140 (▲). The absorbance at 600 nm is plotted versus incubation time. All strains were inoculated directly into the indicated media at an A₆₀₀ of 0.0003 and were not pre-conditioned under iron limitation. **A.** Growth under iron-deficient conditions containing 1 μ M FeCl₃ and 200 μ M dipyrindyl in M9 minimal media. All measurements were performed in triplicate and error bars represent the standard deviation. **B.** Growth under iron-rich conditions containing 200 μ M FeCl₃ in M9 minimal media.

**Scheme 1^a**

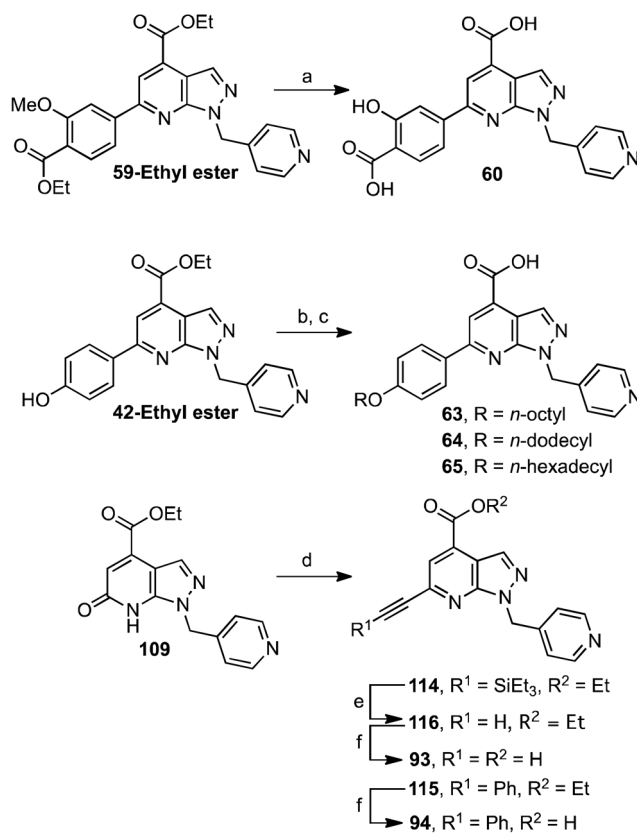
^aReaction conditions: (a) H₂NNH₂·H₂O, EtOH, rt, 24 h; (b) ArCHO, 0 °C to rt, 2 h; (c) *n*-BuONa, *n*-BuOH, 120 °C, 3 h (76%, 3 steps, from **101**); (d) EtO₂C(C=O)CH₂CO₂Et, benzene, 65 °C, 20 h, 48–63%; (e) glacial AcOH, reflux, 3 h, 78–81%.

**Scheme 2^a**

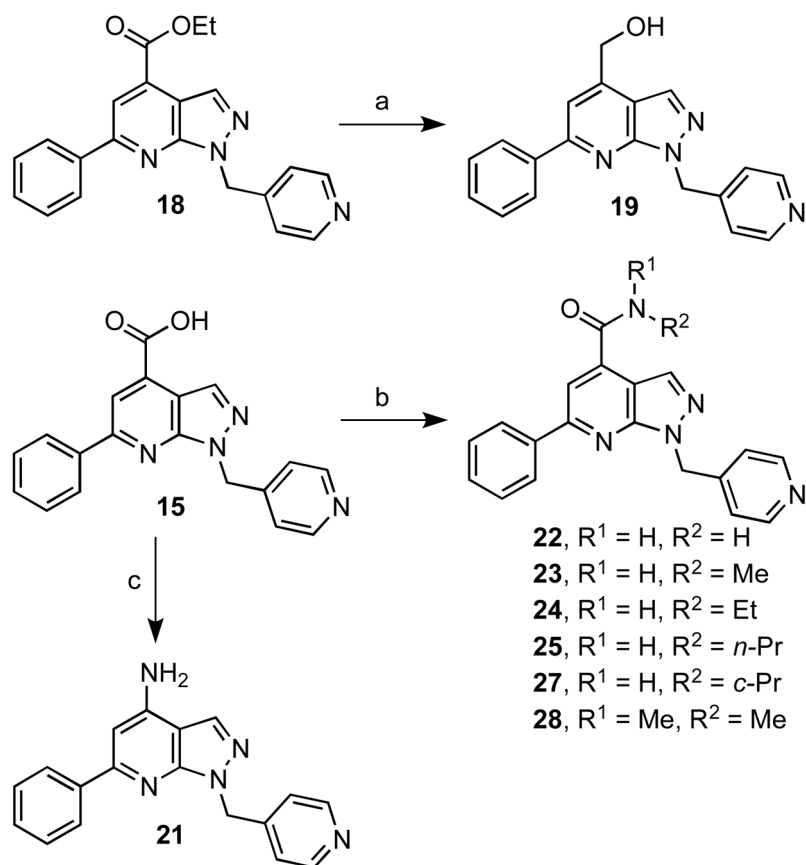
^aReaction conditions: (a) 2,6-di-*t*-butyl-4-methylpyridine, Tf_2O , CH_2Cl_2 , -78 to 0 °C, 4 h, 68%; (b) $\text{Pd}(\text{PPh}_3)_4$, Cs_2CO_3 , $\text{PhB}(\text{OH})_2$, dioxane, 100 °C, 5 h, 96%; (c) TFA, 70 °C, 24 h, 85%; (d) aq. NaOH, THF, rt, 4 h, 84% (average); (e) $(\text{CH}_3)_2\text{S} \cdot \text{BF}_3$, 0 °C to rt, 18 h, 17%; (f) $\text{Pd}(\text{OAc})_2$, BINAP, Cs_2CO_3 , PhNH_2 , dioxane, 100 °C, 22 h, 90%.

**Scheme 3^{a,b}**

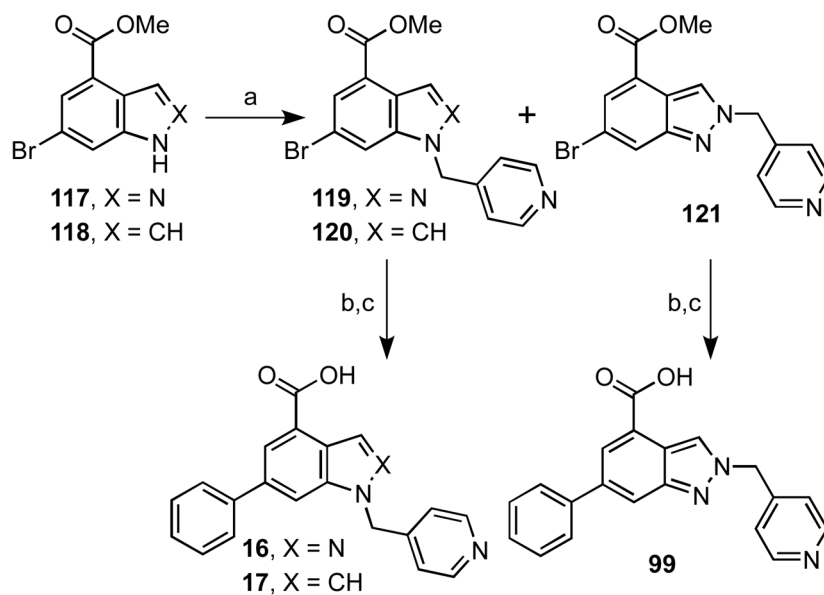
^aReaction conditions: (a) PyBroP, Et₃N, dioxane, rt, 2 h; (b) ArB(OH)₂ or ArB(OH)₂-pinacolate ester, PdCl₂dppf, Na₂CO₃, 5:1 dioxane–H₂O, 100 °C, 4 h, 64% (average, 2 steps, from **109**); (c) aq. NaOH, THF, rt, 4 h, 80% (average); (d) R–C=C–B(OH)₂ or respective pinacolate ester, PdCl₂(PPh₃)₂, Na₂CO₃, 5:1 dioxane–H₂O, 100 °C, 4 h, 76–84% (2 steps, from **109**); (e) BOP, DBU, HNR¹R², dioxane, 70 °C, 5 h, 22–79%. ^bThe structures of **37–59**, **61–62** and **66–90** are shown in Tables 5 and 6.

**Scheme 4^a**

^aReaction conditions: (a) (CH₃)₂S·BF₃, DCM, 0 °C to rt, 3.5 h, 37%; (b) R-Br, Na₂CO₃, dioxane–H₂O, 80 °C, 12 h; (c) NaOH, MeOH, rt, 2 h, 40–70 % (2 steps, from **42-Ethyl ester**); (d) *i*) PyBrOP, Et₃N, dioxane, rt, 2 h; *ii*) R–C≡C–H, PdCl₂(CH₃CN)₂, 2-(dicyclohexylphosphino)biphenyl, Cs₂CO₃, dioxane–H₂O, 85 °C, 6 h, 77–87%; (e) TBAF, THF, 0 °C, 3 h, 35%; (f) NaOH, MeOH, rt, 2 h, 41–65%.

**Scheme 5^a**

^aReaction conditions: (a) LiAlH_4 , THF, 0 °C to rt, 2 h, 48%; (b) *i*) $(\text{COCl})_2$, CH_2Cl_2 , DMF (1 equiv), 0 °C, 1 h; *ii*) HNR^1R^2 , DMAP, rt, 1 h, 39% (average); (c) *i*) $(\text{COCl})_2$, CH_2Cl_2 -THF (3:1), rt, 4 h; *ii*) NaN_3 , acetone- H_2O (1:1); *iii*) TFA, benzene, reflux, 16 h; *iv*) K_2CO_3 , MeOH, rt, 8 h, 31%.

**Scheme 6^a**

^aReaction conditions: (a) Cs₂CO₃, 4-(bromomethyl)pyridine hydrobromide, DMF, rt, 3 h, 50–77%; (b) PdCl₂dppf, Cs₂CO₃, PhB(OH)₂, dioxane, 100 °C, 5 h, 63–77% (c) aq. NaOH, THF, rt, 4 h, 20–77%.

Table 1

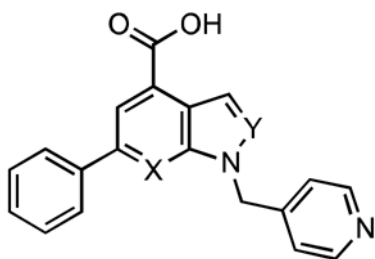
Aryl-capped siderophores producing pathogens and corresponding AAAEs.

	Organism	Siderophore	AAAE	AAAE Substrate^a
Gram-negative	<i>A. baumannii</i>	acinetobactin	BasE	DHB
	<i>E. coli</i>	enterobactin	EntE	DHB
	<i>K. pneumoniae</i>	yersiniabactin	YbtE	DHB
		enterobactin	EntE	SAL
	<i>P. aeruginosa</i>	pyochelin	PchD	DHB
	<i>Y. pestis</i>	yersiniabactin	YbtE	SAL
	<i>Y. pseudotuberculosis</i>	yersiniabactin	YbtE	SAL
	<i>V. cholerae</i>	vibriobactin	VibE	DHB
			VibE1	DHB
<i>V. vulnificus</i>	vulnibactin	VibE2	SAL	
Gram-positive	<i>B. subtilis</i>	bacillibactin	DhbE	DHB
	<i>B. anthracis</i>	petrobactin	AsbC	3,4-DHB
Acid-fast	<i>M. tuberculosis</i>	mycobactin	MbtA	SAL

^aSAL, salicylic acid; DHB, 2,3-dihydroxybenzoic acid; 3-4-DHB, 3,4-dihydroxybenzoic acid

Table 2

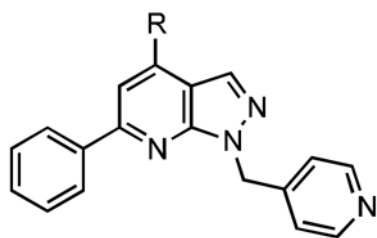
SAR of the core heterocycle.



Compound	X	Y	K_D (nM)	
			BasE	MbtA
15	N	N	36.1 ± 4.9	$(3.74 \pm 0.41) \cdot 10^3$
16	C	N	84.8 ± 10.0	$(27.6 \pm 4.2) \cdot 10^3$
17	C	C	$(52.2 \pm 4.8) \cdot 10^3$	$(161 \pm 7) \cdot 10^3$

Table 3

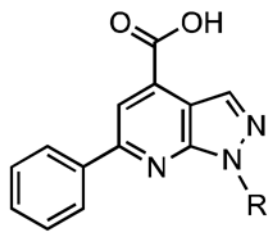
SAR at C-4.



Compound	R	K_D (nM)	
		BasE	MbtA
15	COOH	36.1 ± 4.9	(3.74 ± 0.41)•10 ³
18	COOEt	(2.16 ± 0.30)•10 ³	>100•10 ³
19	CH ₂ OH	102 ± 8	(16.8 ± 4.0)•10 ³
20		>100•10 ³	>100•10 ³
21	NH ₂	200 ± 25	(36.4 ± 7.2)•10 ³
22	CONH ₂	66.8 ± 7.3	(8.57 ± 0.79)•10 ³
23	CONHMe	420 ± 54	>50•10 ³
24	CONHEt	908 ± 69	>50•10 ³
25	CONH(n-Pr)	249 ± 27	>50•10 ³
26	CONH(i-Pr)	164 ± 13	>100•10 ³
27	CONH(c-Pr)	150 ± 19	>100•10 ³
28	CONMe ₂	334 ± 38	>50•10 ³

Table 4

SAR at N-1.



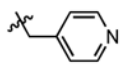
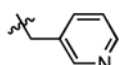
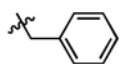
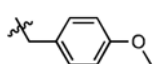
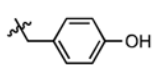
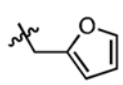

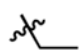
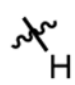
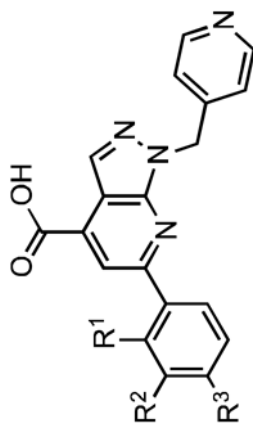
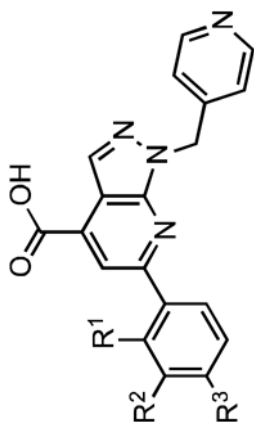
Compound	R	K_D (nM)	
		BasE	MbtA
15		36.1 ± 4.9	$(3.74 \pm 0.41) \cdot 10^3$
29		$>100 \cdot 10^3$	$>100 \cdot 10^3$
30		$>100 \cdot 10^3$	$>100 \cdot 10^3$
31		$>100 \cdot 10^3$	$>100 \cdot 10^3$
32		556 ± 66	$>100 \cdot 10^3$
33		$>100 \cdot 10^3$	$>100 \cdot 10^3$
34		$>500 \cdot 10^3$	$>500 \cdot 10^3$
35		$>500 \cdot 10^3$	$>500 \cdot 10^3$
36		$>100 \cdot 10^3$	$>100 \cdot 10^3$

Table 5

SAR of C-6 phenyl group.

Compound	R ¹	R ²	R ³	K _D (nM)		MbtA
				BaseE	MbtA	
15	H	H	H	36.1 ± 4.9	(3.74 ± 0.41)•10 ³	
37	Me	H	H	(2.15 ± 0.11)•10 ³	>100•10 ³	
38	H	Me	H	158 ± 24	(7.40 ± 0.90)•10 ³	
39	H	H	Me	212 ± 22	(1.44 ± 0.15)•10 ³	
40	OH	H	H	255 ± 36	(6.50 ± 0.90)•10 ³	
41	H	OH	H	124 ± 17	(7.67 ± 1.15)•10 ³	
42	H	H	OH	8.85 ± 3.16	(3.70 ± 0.50)•10 ³	
43	H	H	CH ₂ OH	247 ± 33	(3.70 ± 0.60)•10 ³	
44	Cl	H	H	(2.48 ± 0.19)•10 ³	>100•10 ³	
45	H	Cl	H	2.0	(4.60 ± 0.50)•10 ³	
46	H	H	Cl	153 ± 21	953 ± 90	
47	H	H	Br	20.6 ± 7.0	560 ± 28	
48	H	H	F	28 ± 4.7	(1.89 ± 0.21)•10 ³	
49	F	H	F	42.6 ± 8.3	(8.00 ± 0.90)•10 ³	
50	H	H	CF ₃	191 ± 27	887 ± 96	
51	H	H	NO ₂	3.91 ± 2.27	202 ± 38	
52	H	H	NH ₂	78.2 ± 13.2	(4.08 ± 0.63)•10 ³	
53	H	H	N(Me) ₂	628 ± 98	(1.70 ± 0.30)•10 ³	

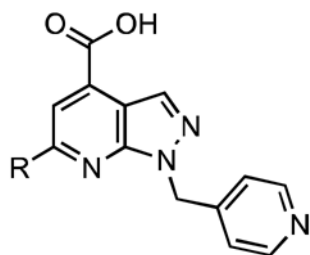




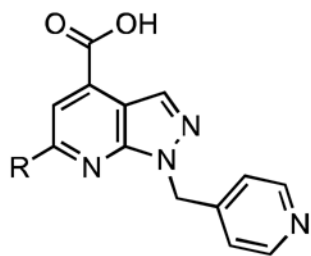
Compound	R ¹	R ²	R ³	K _D (nM)		MbitA
				BaseE		
54	H	H	NH(C=O)Me	747 ± 65	(4.20 ± 0.80)•10 ³	130 ± 23
55	H	H	SO ₂ Me	13.0 ± 6.1		380 ± 46
56	H	H	CN	22.7 ± 6.2		
57	H	H	C(=O)NH ₂	288 ± 45	(1.00 ± 0.30)•10 ³	
58	H	H	COOH	776 ± 119	(6.10 ± 0.80)•10 ³	
59	H	OMe	COOH	(1.70 ± 0.15)•10 ³	(49.9 ± 3.7)•10 ³	
60	H	OH	COOH	169 ± 13.4		495 ± 34
61	H	H	SMe	23.5 ± 5.5		178 ± 15
62	H	H	OMe	78.2 ± 13.2	(3.23 ± 0.38)•10 ³	
63	H	H	O(CH ₂) ₇ CH ₃	191 ± 13		>50•10 ³
64	H	H	O(CH ₂) ₁₁ CH ₃	(28.4 ± 3.9)•10 ³		>50•10 ³
65	H	H	O(CH ₂) ₁₅ CH ₃	-		-
66	H	H	OPh	32.5 ± 6.3		187 ± 28
67	H	H	OCH ₂ Ph	2.14 ± 1.46	(5.40 ± 0.90)•10 ³	
68	H	H	OCH ₂ (p-PhOMe)	44.5 ± 7.7	(5.80 ± 0.90)•10 ³	
69	H	H	C(=O)Me	104 ± 11		134 ± 22
70	H	H	C(=O)Ph	19.1 ± 4.9		19.1 ± 2.4
71	H	Ph	H	164 ± 20	(3.60 ± 0.38)•10 ³	
72	H	H	Ph	125 ± 9	(3.50 ± 0.30)•10 ³	
73	H	H	p-PhBr	181 ± 39	(19.7 ± 0.9)•10 ³	
74	o-PhCl	H	H	(19.7 ± 0.9)•10 ³		>50•10 ³

Table 6

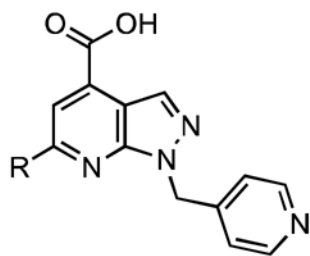
SAR at C-6: substitution with heterocycles, alkynes, alkenes, and amines.



Entry	R	K_D (nM)	
		BasE	MbtA
15	Ph	36.1 ± 4.9	$(3.74 \pm 0.41) \cdot 10^3$
75		342 ± 53	$(19.5 \pm 2.2) \cdot 10^3$
76		443 ± 74	$(6.68 \pm 0.50) \cdot 10^3$
77		340 ± 32	$(19.2 \pm 1.7) \cdot 10^3$
78		86.9 ± 18.7	$(2.54 \pm 0.41) \cdot 10^3$
79		7.60 ± 2.49	$(2.60 \pm 0.60) \cdot 10^3$
80		36.3 ± 7.5	318 ± 56
81		62.4 ± 8.5	701 ± 163



Entry	R	K_D (nM)	
		BasE	MbtA
82		39.2 ± 7.5	264 ± 30
83		132 ± 16	$(16.8 \pm 1.7) \cdot 10^3$
84		121 ± 19	901 ± 109
85		$(1.17 \pm 0.14) \cdot 10^3$	380 ± 35
86		$(7.73 \pm 0.43) \cdot 10^3$	$> 100 \cdot 10^3$
87		61.8 ± 10.4	$(2.90 \pm 0.20) \cdot 10^3$
88		776 ± 52	$(22.5 \pm 2.1) \cdot 10^3$
89		583 ± 44	$(13.6 \pm 0.7) \cdot 10^3$



Entry	R	K_D (nM)	
		BasE	MbtA
90		$(2.30 \pm 0.20) \cdot 10^3$	$(27.9 \pm 1.6) \cdot 10^3$
91		$(1.90 \pm 0.20) \cdot 10^3$	$> 100 \cdot 10^3$
92		280 ± 43	$(5.10 \pm 0.70) \cdot 10^3$
93		$(2.04 \pm 0.20) \cdot 10^3$	$(18.5 \pm 2.0) \cdot 10^3$
94		421 ± 61	$(3.00 \pm 0.60) \cdot 10^3$
95		$(2.32 \pm 0.29) \cdot 10^3$	$(6.02 \pm 0.72) \cdot 10^3$
96		$(1.45 \pm 0.16) \cdot 10^3$	$(29.1 \pm 2.0) \cdot 10^3$
97		$(2.46 \pm 0.24) \cdot 10^3$	$(97.7 \pm 9.8) \cdot 10^3$
98		$> 100 \cdot 10^3$	$> 100 \cdot 10^3$

Table 7

Miscellaneous SAR.

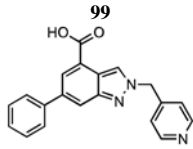
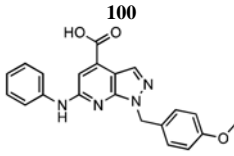
Compound	K_D (nM)	
	BasE	MbtA
<p>99</p> 	$(66.4 \pm 6.3) \cdot 10^3$	$(58.0 \pm 4.1) \cdot 10^3$
<p>100</p> 	$> 100 \cdot 10^3$	$> 100 \cdot 10^3$

Table 8

Crystallographic Diffraction and Refinement data.

	BasE • 67	BasE • 70
PDB Accession Code	3U16	3U17
Resolution	40.0 – 2.1 Å	50.0 – 2.1 Å
Space Group	P2 ₁ 2 ₁ 2 ₁	P2 ₁ 2 ₁ 2 ₁
Unit Cell	a=66.1 Å b=144.8 Å c=148.7 Å	a=65.5 Å b=143.3 Å c=148.8 Å
R _{merge} ^a	10.2 % (54.2%)	7.0 % (34.2 %)
Completeness ^a	98.0 % (88.4%)	90.2 % (51.9 %)
I/s ^a	11.8	10.1
# Observations	365612	280779
# Reflections	82980	74749
R _{cryst} (Overall/Highest Resolution Shell) ^a	18.5 % (26.8 %)	19.0 % (26.7 %)
R _{free} (Overall/Highest Resolution Shell) ^a	21.9 % (31.9 %)	22.1 % (31.0 %)
Wilson B-factor	32.1 Å ²	28.9 Å ²
Average B-Factor, Protein ^b	A=36.6 Å ² B=36.8 Å ²	A=41.3 Å ² B=41.2 Å ²
Average B-Factor, Ligand, Solvent, Ions (Å ²)	34.4, 39.9, 46.6	34.9, 41.5, 55.5
Number of Water Molecules, Ions	511 H ₂ O, 6 Ca ²⁺ ions	379 H ₂ O, 1 Ca ²⁺ ion
RMS Deviation Bond Lengths, Angles	0.007 Å, 1.06°	0.007 Å, 1.05°

^aValues for the highest resolution shell are given in parentheses.

Table 9MIC₉₉ determined against *M. tuberculosis* H37Rv (μM).

Compound	MIC (μM)	
	Iron-deficient (GAST/-Fe)	Iron-replete (GAST/+Fe)
15	>125	>125
18	>125	125
66	25	25
66-ethyl ester	50	100
70	>125	>125
70-ethyl ester	>125	>125
82	50	50
82-ethyl ester	25	25